

ARCS: Accurate Rotation and Correspondence Search

Liangzu Peng
Johns Hopkins University
lpeng25@jhu.edu

Manolis C. Tsakiris
ShanghaiTech University
mtsakiris@shanghaitech.edu.cn

René Vidal
Johns Hopkins University
rvidal@jhu.edu

Abstract

This paper is about the old Wahba problem in its more general form, which we call “simultaneous rotation and correspondence search”. In this generalization we need to find a rotation that best aligns two partially overlapping 3D point sets, of sizes m and n respectively with $m \geq n$. We first propose a solver, ARCS, that i) assumes noiseless point sets in general position, ii) requires only 2 inliers, iii) uses $O(m \log m)$ time and $O(m)$ space, and iv) can successfully solve the problem even with, e.g., $m, n \approx 10^6$ in about 0.1 seconds. We next robustify ARCS to noise, for which we approximately solve consensus maximization problems using ideas from robust subspace learning and interval stabbing. Thirdly, we refine the approximately found consensus set by a Riemannian subgradient descent approach over the space of unit quaternions, which we show converges globally to an ε -stationary point in $O(\varepsilon^{-4})$ iterations, or locally to the ground-truth at a linear rate in the absence of noise. We combine these algorithms into ARCS+, to simultaneously search for rotations and correspondences. Experiments show that ARCS+ achieves state-of-the-art performance on large-scale datasets with more than 10^6 points with a 10^4 time-speedup over alternative methods. <https://github.com/liangzu/ARCS>

1. Introduction

The villain Procrustes forced his victims to sleep on an iron bed; if they did not fit the bed he cut off or stretched their limbs to make them fit [32].

Richard Everson

Modern sensors have brought the classic Wahba problem [86], or slightly differently the Procrustes analysis problem [36], into greater generality that has increasing importance to computer vision [39, 57], computer graphics [65], and robotics [14]. We formalize this generalization as follows.

Problem 1 (simultaneous rotation and correspondence

search). Consider point sets $\mathcal{Q} = \{\mathbf{q}_1, \dots, \mathbf{q}_m\} \subset \mathbb{R}^3$ and $\mathcal{P} = \{\mathbf{p}_1, \dots, \mathbf{p}_n\} \subset \mathbb{R}^3$ with $m \geq n$. Let \mathcal{C}^* be a subset of $[m] \times [n] := \{1, \dots, m\} \times \{1, \dots, n\}$ of size k^* , called the inlier correspondence set, such that all pairs (i_1, j_1) and (i_2, j_2) of \mathcal{C}^* satisfy $i_1 \neq i_2$ and $j_1 \neq j_2$. Assume that

$$\mathbf{q}_i = \mathbf{R}^* \mathbf{p}_j + \boldsymbol{\epsilon}_{i,j}, \quad \text{if } (i, j) \in \mathcal{C}^* \quad (1)$$

where $\boldsymbol{\epsilon}_{i,j} \sim \mathcal{N}(0, \sigma^2 \mathbf{I}_3)$ is noise, \mathbf{R}^* is an unknown 3D rotation, and $(\mathbf{q}_i, \mathbf{p}_j)$ is called an inlier. If $(i, j) \notin \mathcal{C}^*$ then $(\mathbf{q}_i, \mathbf{p}_j)$ is arbitrary and is called an outlier. The goal of the simultaneous rotation and correspondence search problem is to simultaneously estimate the 3D rotation \mathbf{R}^* and the inlier correspondence set \mathcal{C}^* from point sets \mathcal{Q} and \mathcal{P} .

We focus on Problem 1 for two reasons. First, it already encompasses several vision applications such as image stitching [19]. Second, the more general and more important simultaneous pose and correspondence problem, which involves an extra unknown translation in (1), reduces to Problem 1 by eliminating the translation parameters (at the cost of squaring the number of measurements) [91]. As surveyed in [43], whether accurate and fast algorithms exist for solving the pose and correspondence search is largely an open question. Therefore, solving the simpler Problem 1 efficiently is an important step for moving forward.

For Problem 1 or its variants, there is a vast literature of algorithms that are based on i) local optimization via iterative closest points (ICP) [15, 23, 76] or graduated non-convexity (GNC) [2, 87, 96] or others [26, 46, 68], ii) global optimization by branch & bound [21, 24, 57, 61, 62, 73, 80, 92], iii) outlier removal techniques [19, 71, 72, 79, 91], iv) semidefinite programming [44, 65, 81, 88, 90], v) RANSAC [33, 58, 59, 82], vi) deep learning [5, 10, 25, 42], and vii) spherical Fourier transform [14]. But all these methods, if able to accurately solve Problem 1 with the number k^* of inliers extremely small, take $\Omega(mn)$ time. Yet we have:

Theorem 1 (ARCS). *Suppose there are at least two inliers, $k^* \geq 2$, and that the point sets \mathcal{Q} and \mathcal{P} of Problem 1 are noiseless “in general position”. Then there is an algorithm that solves Problem 1 in $O(m \log m)$ time and $O(m)$ space.*

Remark 1 (general position assumption). In Theorem 1, by “in general position” we mean that i) for any outlier $(\mathbf{q}_i, \mathbf{p}_j)$, we have $\|\mathbf{q}_i\|_2 \neq \|\mathbf{p}_j\|_2$, ii) there exists some inlier pairs $(\mathbf{q}_{i_1}, \mathbf{p}_{j_1})$ and $(\mathbf{q}_{i_2}, \mathbf{p}_{j_2})$ such that \mathbf{q}_{i_1} and \mathbf{q}_{i_2} are not parallel. If point sets \mathcal{Q} and \mathcal{P} are randomly sampled from \mathbb{R}^3 , these two conditions hold true with probability 1.

A numerical illustration of Theorem 1 is that our ARCS solver, to be described in §3, can handle the case where $m = 10^6$, $n = 8 \times 10^5$ and $k^* = 2$, in about 0.1 seconds (cf. Table 1).¹ However, like other correspondence-based minimal solvers for geometric vision [34, 51–53, 70], ARCS might be fragile to noise. That being said, it can be extended to the noisy case, leading to a three-step algorithm called ARCS+, which we summarize next.

The first step ARCS+N of ARCS+ extends ARCS by *establishing correspondences under noise*. ARCS+N outputs in $O(\ell + m \log m)$ time a candidate correspondence set $\hat{\mathcal{C}}$ of size ℓ that contains \mathcal{C}^* . Problem 1 then reduces to estimating \mathbf{R}^* and \mathcal{C}^* from \mathcal{P} , \mathcal{Q} , and hypothetical correspondences $\hat{\mathcal{C}}$, a simpler task of *robust rotation search* [19, 72, 88, 96].

The second step ARCS+O of ARCS+ is to *remove outliers* from the previous step 1. To do so we approximately maximize an appropriate consensus over $\text{SO}(3)$ (§4.2). Instead of mining inliers in $\text{SO}(3)$ [11, 39, 48, 57, 73], we show that the parameter space of consensus maximization can be reduced from $\text{SO}(3)$ to \mathbb{S}^2 and further to $[0, \pi]$ (see [19] for a different reduction). With this reduction, ARCS+O removes outliers via repeatedly solving in $O(\ell \log \ell)$ time a computational geometry problem, *interval stabbing* [28] (§4.2.1). Note that ARCS+O only repeats for $s \approx 90$ times to reach satisfactory accuracy. Therefore, conceptually, for $\ell \geq 10^6$, it is 10^4 times faster than the most related outlier removal method GORE [19], which uses $O(\ell^2 \log \ell)$ time (Table 4).

The third and final step ARCS+R of our ARCS+ pipeline is to accurately estimate the rotation, using the consensus set from the second step (§4.3). In short, ARCS+R is a *Riemannian subgradient descent* method. Our novelty here is to descend in the space \mathbb{S}^3 of unit quaternions, not $\text{SO}(3)$ [16]. This allows us to derive, based on [60], that ARCS+R converges linearly though locally to the ground-truth unit quaternion, thus obtaining the first to our knowledge convergence rate guarantee for robust rotation search.

Numerical highlights are in order (§5). ARCS+O is an outlier pruning procedure for robust rotation search that can handle extremely small inlier ratios $k^*/\ell = 3000/10^7 = 0.03\%$ in 5 minutes; ARCS+O + ARCS+R, or ARCS+OR for short, accurately solves the robust rotation search problem with $k^*/\ell = 10^3/10^6$ in 23 seconds (see Table 4). ARCS+N + ARCS+OR, that is ARCS+, solves Problem 1 with $m = 10^4$, $n = 8000$, $k^* = 2000$ in 90 seconds (see Figure 2). To the best of our knowledge, all these challenging cases

have not been considered in prior works. In fact, as we will review soon (§2), applying state-of-the-art methods to those cases either gives wrong estimates of rotations, or takes too much time (≥ 8 hours), or exhausts the memory (Table 4).

2. Prior Art: Accuracy Versus Scalability

Early efforts on Problem 1 have encountered an *accuracy versus scalability* dilemma. The now classic ICP algorithm [15] estimates the rotation and correspondences in an alternating fashion, running in real time but requiring a high-quality and typically unavailable initialization to avoid local and usually poor minima; the same is true for its successors [23, 26, 46, 68, 76]. The GO-ICP method [92, 93] of the branch & bound type enumerates initializations fed to ICP to reach a global minimum—in exponential time; the same running time bound is true for its successors [21, 62, 73].

The above ICP versus GO-ICP dilemma was somewhat alleviated by a two-step procedure: i) compute a candidate correspondence set $\hat{\mathcal{C}}$, via hand-crafted [77] or learned [35] feature descriptors, and ii) estimate the rotation from point sets indexed by $\hat{\mathcal{C}}$. But, as observed in [91], due to the quality of the feature descriptors, there could be fewer than 2 inliers remaining in $\hat{\mathcal{C}}$, from which the ground-truth rotation can never be determined. An alternative and more conservative idea is to use *all-to-all* correspondences $\hat{\mathcal{C}} := [m] \times [n]$, although now the inlier ratio becomes extremely small.

This justifies why researchers have recently focused on designing robust rotation search algorithms for extreme outlier rates, e.g., ≥ 90 outliers out of 100. One such design is GORE [19], a guaranteed outlier removal algorithm of $O(\ell^2 \log \ell)$ time complexity that heavily exploits the geometry of $\text{SO}(3)$. The other one is the semidefinite relaxation QUASAR of [88], which involves sophisticated manipulation on unit quaternions; $\ell \approx 1000$ constitutes the current limit on the number of points this relaxation can handle. Yet another one is TEASER++ [91]; its robustness to outliers comes mainly from finding via parallel branch & bound [75] a maximum clique of the graph whose vertices represent point pairs and whose edges indicate whether two point pairs can simultaneously be inliers. This maximum clique formulation was also explored by [71] where it was solved via a different branch & bound algorithm. Since finding a maximum clique is in general NP-hard, their algorithms take exponential time in the worst case; in addition, TEASER++ was implemented to trade $O(\ell^2)$ space for speed. One should also note though that if noise is small then the graph is sparse so that the otherwise intractable branch & bound algorithm can be efficient. Since constructing such a graph entails checking $\binom{\ell}{2}$ point pairs, recent follow-up works [58, 63, 79, 81, 82] that use such a graph entail $O(\ell^2)$ time complexity. While all these methods are more accurate than scalable, the following two are on the other side. FGR [96] combines *graduated non-convexity*

¹We run experiments on an Intel(R) i7-1165G7, 16GB laptop. In the paper we consider random instead of adversarial outliers.

(GNC) and alternating minimization, while GNC-TLS [87] combines *truncated least squares*, iteratively reweighted least-squares, and GNC. Both of them scale gracefully with ℓ , while being robust against up to $80/100 = 80\%$ outliers.

Is such accuracy versus scalability dilemma of an inherent nature of the problems here, or can we escape from it?

3. ARCS: Accuracy & Scalability

Basic Idea. Although perhaps not explicitly mentioned in the literature, it should be known that there is a simple algorithm that solves Problem 1 under the assumptions of Theorem 1. This algorithm first computes the ℓ_2 norm of each point in \mathcal{Q} and \mathcal{P} and the difference $d_{i,j} := \|\mathbf{q}_i\|_2 - \|\mathbf{p}_j\|_2$. Since \mathcal{Q} and \mathcal{P} are in general position (Remark 1), we have that $(\mathbf{q}_i, \mathbf{p}_j)$ is an inlier pair if and only if $d_{i,j} = 0$. Based on the $d_{i,j}$'s, extract all such inlier pairs. Since $k^* \geq 2$, and by the general position assumption (Remark 1), there exist two inlier pairs say $(\mathbf{q}_1, \mathbf{p}_1), (\mathbf{q}_2, \mathbf{p}_2)$ such that \mathbf{q}_1 and \mathbf{q}_2 are not parallel. As a result and as it has been well-known since the 1980's [4, 40, 41, 64], if not even earlier [78, 86], \mathbf{R}^* can be determined from the two inlier pairs by SVD.

ARCS: Efficient Implementation. Not all the $d_{i,j}$'s should be computed in order to find the correspondence set \mathcal{C}^* , meaning that the otherwise $O(mn)$ time complexity can be reduced. Our ARCS Algorithm 1 seeks all point pairs $(\mathbf{q}_i, \mathbf{p}_j)$'s whose norms are close, *i.e.*, they satisfy $|d_{i,j}| \leq c$, for some sufficiently small $c \geq 0$. Here c is provided as an input of ARCS and set as 0 in the current context. It is clear that, under the general position assumption of Theorem 1, the set $\bar{\mathcal{C}}$ returned by ARCS is exactly the ground-truth correspondence set \mathcal{C}^* . It is also clear that ARCS takes $O(m \log m)$ time and $O(m)$ space (recall $m \geq n \geq |\mathcal{C}^*|$).

We proved Theorem 1. It is operating in the noiseless case that allows us to show that Problem 1 can be solved accurately and at large scale. Indeed, ARCS can handle more than 10^6 points with $k^* = 2$ in about 0.1 seconds, even though generating those points has taken more than 0.2 seconds, as shown in Table 1.² Note that in the setting of Table 1 we have only $k^* = 2$ overlapping points, a situation where all prior methods mentioned in §1 and §2, if directly applicable, in principle break down. One reason is that they are not designed to handle the noiseless case. The other reason is that the overlapping ratio k^*/m of Table 1 is the minimum possible. While the achievement in Table 1 is currently limited to the noiseless case, it forms a strong motivation that urges us to robustify ARCS to noise, while keeping as much of its accuracy and scalability as possible. Such robustification is the main theme of the next section.

²For experiments in Tables 1 and 2 we generate data as per Section 5.1.

Algorithm 1: ARCS

```

1 Input:  $\mathcal{Q} = \{\mathbf{q}_i\}_{i=1}^m, \mathcal{P} = \{\mathbf{p}_j\}_{j=1}^n, c \geq 0$ ;
2 Sort  $\mathcal{Q}$  so that (w.l.o.g.)  $\|\mathbf{q}_1\|_2 \leq \dots \leq \|\mathbf{q}_m\|_2$ ;
3 Sort  $\mathcal{P}$  so that (w.l.o.g.)  $\|\mathbf{p}_1\|_2 \leq \dots \leq \|\mathbf{p}_n\|_2$ ;
4  $i = 1; j = 1; \bar{\mathcal{C}} = \emptyset$ ;
5 while  $i \leq m$  and  $j \leq n$  do
6    $d_{i,j} \leftarrow \|\mathbf{q}_i\|_2 - \|\mathbf{p}_j\|_2$ ;
7   if  $d_{i,j} > c$  then
8      $j \leftarrow j + 1$ ;
9   end
10  if  $d_{i,j} < -c$  then
11     $i \leftarrow i + 1$ ;
12  end
13  if  $-c \leq d_{i,j} \leq c$  then
14     $\bar{\mathcal{C}} \leftarrow \bar{\mathcal{C}} \cup (i, j); (i, j) \leftarrow (i + 1, j + 1)$ ;
15  end
16 end
17 return  $\bar{\mathcal{C}}$ ;

```

Table 1. Time (msec) of generating noiseless Gaussian point sets (G) and solving Problem 1 by ARCS (100 trials, $k^* = 2$).

	m	10^4	10^5	10^6
	n	8×10^3	8×10^4	8×10^5
G		5.9	15.0	212.8
Brute Force		73.8	8304	8380441.5
ARCS		1.51	8.4	121.1

4. ARCS+: Robustifying ARCS to Noise

Here we consider Problem 1 with noise $\epsilon_{i,j}$. We will illustrate our algorithmic ideas by assuming $\epsilon_{i,j} \sim \mathcal{N}(0, \sigma^2 \mathbf{I}_3)$, although this is not necessary for actual implementation. As indicated in §1, ARCS+ has three steps. We introduce them respectively in the next three subsections.

4.1. Step 1: Finding Correspondences Under Noise

A simple probability fact is $\|\mathbf{q}_i - \mathbf{R}^* \mathbf{p}_j\|_2 \leq 5.54\sigma$ for any inlier $(\mathbf{q}_i, \mathbf{p}_j)$, so $|d_{i,j}| \leq 5.54\sigma$ with probability at least $1 - 10^{-6}$ (see, *e.g.*, [91]). To establish correspondences under noise, we need to modify³ the while loop of Algorithm 1, such that, in $O(\ell + m \log m)$ time, it returns the set $\bar{\mathcal{C}}$ of all correspondences of size ℓ where each $(i, j) \in \bar{\mathcal{C}}$ satisfies $|d_{i,j}| \leq c$, with c now set to 5.54σ . Note that, to store the output correspondences, we need an extra $O(\ell)$ time, which can not be simply ignored as ℓ is in general larger than m in the presence of noise (Table 2). We call this modified version ARCS+_N. ARCS+_N gives a set $\bar{\mathcal{C}}$ that

³The details of this modification can be found at: https://github.com/liangzu/ARCS/blob/main/ARCSplus_N.m

Table 2. The number ℓ of candidate correspondences produced by ARCS+_N on synthetic noisy Gaussian point sets. A single trial.

m	1000	5000	10000
n	800	4000	8000
k^*	200	1000	2000
ℓ	36622	931208	3762888
$\ell/(mn)$	4.58%	4.66%	4.70%

contains all inlier correspondences \mathcal{C}^* with probability at least $(1 - 10^{-6})^{k^*}$. This probability is larger than 99.9% if $k^* \leq 10^3$, or larger than 99% if $k^* \leq 10^4$.

Remark 2 (feature matching versus all-to-all correspondences versus ARCS+_N). Feature matching methods provide fewer than n hypothetical correspondences and thus speed up the subsequent computation, but they might give no inliers. Using all-to-all correspondences preserves all inliers, but a naive computation needs $O(mn)$ time and leads to a large-scale problem with extreme outlier rates. ARCS+_N strikes a balance by delivering in $O(\ell + m \log m)$ time a candidate correspondence set \mathcal{C} of size ℓ containing all inliers with high probability and with $\ell \ll mn$.

For illustration, Table 2 reports the number ℓ of correspondences that ARCS+_N typically yields. As shown, even though $\ell/(mn)$ is usually smaller than 5%, yet ℓ itself could be very large, and the inlier ratio k^*/ℓ is extremely small (e.g., $\leq 0.05\%$). This is perhaps the best we could do for the current stage, because for now we only considered every point pair individually, while any pair (q_i, p_i) is a potential inlier if it satisfies the necessary (but no longer sufficient) condition $|d_{i,j}| \leq c$. On the other hand, collectively analyzing the remaining point pairs allows to further remove outliers, and this is the major task of our next stage (§4.2).

4.2. Step 2: Outlier Removal

Let there be some correspondences given, by, e.g., either ARCS+_N or feature matching (cf. Remark 2). Then we arrive at an important special case of Problem 1, called *robust rotation search*. For convenience we formalize it below:

Problem 2. (robust rotation search) Consider ℓ pairs of 3D points $\{(\mathbf{y}_i, \mathbf{x}_i)\}_{i=1}^{\ell}$, with each pair satisfying

$$\mathbf{y}_i = \mathbf{R}^* \mathbf{x}_i + \mathbf{o}_i + \boldsymbol{\epsilon}_i. \quad (2)$$

Here $\boldsymbol{\epsilon}_i \sim \mathcal{N}(0, \sigma^2 \mathbf{I}_3)$ is noise, $\mathbf{o}_i = \mathbf{0}$ if $i \in \mathcal{I}^*$ where $\mathcal{I}^* \subset [\ell]$ is of size k^* , and if $i \notin \mathcal{I}^*$ then \mathbf{o}_i is nonzero and arbitrary. The task is to find \mathbf{R}^* and \mathcal{I}^* .

The percentage of outliers in Problem 2 can be quite large (cf. Table 2), so our second step ARCS+_O here is to remove outliers. In §4.2.1, we shortly review the interval stabbing problem, on which ARCS+_O of §4.2.2 is based.

4.2.1 Preliminaries: Interval Stabbing

Consider a collection of subsets of \mathbb{R} , $\{\mathcal{J}_i\}_{i=1}^L$, where each \mathcal{J}_i is an interval of the form $[a, b]$. In the interval stabbing problem, one needs to determine a point $\omega \in \mathbb{R}$ and a subset \mathcal{I} of $\{\mathcal{J}_i\}_{i=1}^L$, so that \mathcal{I} is a maximal subset whose intervals overlap at ω . Formally, we need to solve

$$\begin{aligned} & \max_{\mathcal{I} \subset [L], \omega \in \mathbb{R}} |\mathcal{I}| \\ \text{s.t. } & \omega \in \mathcal{J}_i, \forall i \in \mathcal{I} \end{aligned} \quad (3)$$

For this purpose, the following result is known.

Lemma 1 (interval stabbing). *Problem (3) can be solved in $O(L \log L)$ time and $O(L)$ space.*

Actually, the interval stabbing problem can be solved using sophisticated data structures such as *interval tree* [28] or *interval skip list* [37]. On the other hand, it is a basic exercise to find an algorithm that solves Problem (3), which, though also in $O(L \log L)$ time, involves only a sorting operation and a for loop (details are omitted, see, e.g., [20]). Finally, note that the use of interval stabbing for robust rotation search is not novel, and can be found in GORE [19, 72]. However, as the reader might realize after §4.2.2, our use of interval stabbing is quite different from GORE.

4.2.2 The Outlier Removal Algorithm

We now consider the following consensus maximization:

$$\begin{aligned} & \max_{\mathcal{I} \subset [\ell], \mathbf{R} \in \text{SO}(3)} |\mathcal{I}| \\ \text{s.t. } & \|\mathbf{y}_i - \mathbf{R} \mathbf{x}_i\|_2 \leq c, \forall i \in \mathcal{I}. \end{aligned} \quad (4)$$

It has been shown in [84] that for the very related *robust fitting* problem, such consensus maximization is in general NP-hard⁴. Thus it seems only prudent to switch our computational goal from solving (4) exactly to approximately.

From SO(3) to \mathbb{S}^2 . Towards this goal, we first shift our attention to \mathbb{S}^2 where the rotation axis \mathbf{b}^* of \mathbf{R}^* lives. An interesting observation is that the axis \mathbf{b}^* has the following interplay with data, independent of the rotation angle of \mathbf{R}^* .

Proposition 1. *Let $\mathbf{v}_i := \mathbf{y}_i - \mathbf{x}_i$. Recall $\boldsymbol{\epsilon}_i \sim \mathcal{N}(0, \sigma^2 \mathbf{I}_3)$. If $(\mathbf{y}_i, \mathbf{x}_i)$ is an inlier pair, then $\mathbf{v}_i^\top \mathbf{b}^* \sim \mathcal{N}(0, \sigma^2)$, and so $|\mathbf{v}_i^\top \mathbf{b}^*| \leq 4.9\sigma$ with probability at least $1 - 10^{-6}$.*

Proposition 1 (cf. Appendix C) leads us to Problem (5):

$$\begin{aligned} & \max_{\mathcal{I} \subset [\ell], \mathbf{b} \in \mathbb{S}^2} |\mathcal{I}| \\ \text{s.t. } & |\mathbf{v}_i^\top \mathbf{b}| \leq \bar{c}, \forall i \in \mathcal{I} \\ & b_2 \geq 0. \end{aligned} \quad (5)$$

⁴Interestingly, consensus maximization over SO(2), i.e., the 2D version of (4), can be solved in $O(\ell \log \ell)$ time; see [20].

In (5) the constraint on the second entry b_2 of \mathbf{b} is to eliminate the symmetry, and Proposition 1 suggests to set $\bar{c} := 4.9\sigma$. Problem (5) is easier than (4) as it has fewer degrees of freedom; see also [19] where a different reduction to a 2 DoF (sub-)problem was derived for GORE.

Solving (5) is expected to yield an accurate estimate of \mathbf{b}^* , from which the rotation angle can later be estimated. Problem (5) reads: find a plane (defined by the normal \mathbf{b}) that approximately contains as much points \mathbf{v}_i 's as possible. This is an instance of the *robust subspace learning* problem [30, 31, 54, 85, 94, 97, 98], for which various scalable algorithms with strong theoretical guarantees have been developed in more tractable formulations (e.g., ℓ_1 minimization) than consensus maximization. Most notably, the so-called *dual principal component pursuit* formulation [85] was proved in [98] to be able to tolerate $O((k^*)^2)$ outliers. Still, all these methods can not handle as many outliers as we currently have (cf. Table 2), even though they can often minimize their objective functions to global optimality.

From \mathbb{S}^2 to $[0, \pi]$. We can further “reduce” the degrees of freedom in (5) by 1, through the following lens. Certainly $\mathbf{b} \in \mathbb{S}^2$ in (5) is determined by two angles $\theta \in [0, \pi]$, $\phi \in [0, \pi]$. Now consider the following problem:

$$\begin{aligned} & \max_{\mathcal{I} \subset [\ell], \theta \in [0, \pi]} |\mathcal{I}| \\ \text{s.t.} \quad & |\mathbf{v}_i^\top \mathbf{b}| \leq \bar{c}, \quad \forall i \in \mathcal{I} \\ & \mathbf{b} = [\sin(\theta) \cos(\phi), \sin(\theta) \sin(\phi), \cos(\theta)]^\top. \end{aligned} \quad (6)$$

Problem (6) is a simplified version of (5) with ϕ given. Clearly, to solve (5) it suffices to minimize the function $f : [0, \pi] \rightarrow \mathbb{R}$ which maps any $\phi_0 \in [0, \pi]$ to the objective value of (6) with $\phi = \phi_0$. Moreover, we have:

Proposition 2. *Problem (6) can be solved in $O(\ell \log \ell)$ time and $O(\ell)$ space via interval stabbing.*

Proposition 2 gives an $O(\ell \log \ell)$ time oracle to access the values of f . Since computing the objective value of (5) given θ, ϕ already needs $O(\ell)$ time, the extra cost of the logarithmic factor in Proposition 2 is nearly negligible. Since f has only one degree of freedom, its global minimizer can be found by *one-dimensional branch & bound* [47]. But this entails exponential time complexity in the worst case, a situation we wish to sidestep. Alternatively, the search space $[0, \pi]$ is now so small that the following algorithm ARCS+_o turns out to be surprisingly efficient and robust: i) *sampling* from $[0, \pi]$, ii) *stabbing* in \mathbb{S}^2 , and iii) *stabbing* in $\text{SO}(3)$.

Sampling from $[0, \pi]$. Take s equally spaced points $\phi_j = (2j-1)\pi/(2s), \forall j \in [s]$, on $[0, \pi]$. The reader may find this choice of ϕ_j 's similar to the *uniform grid approach* [69]; in the latter Nesterov commented that “the reason why it works here is related to the *dimension* of the problem”.

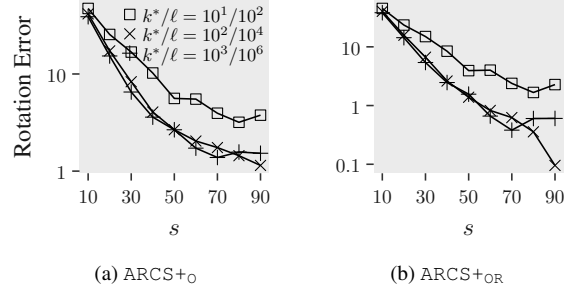


Figure 1. Rotation errors (in degrees) of steps 2 and 3 for robust rotation search methods with s varying (500 trials, $\sigma = 0.01$).

Stabbing in \mathbb{S}^2 . For each $j \in [s]$, solve (6) with $\phi = \phi_j$ to get s candidate consensus set \mathcal{I}_j 's and s angles θ_j 's. From each ϕ_j and θ_j we obtain a candidate rotation axis \mathbf{b}_j .

Stabbing in $\text{SO}(3)$. Since now we have estimates of rotation axes, \mathbf{b}_j 's, there is one degree of freedom remaining, the rotation angle ω . For this we consider:

$$\begin{aligned} & \max_{\mathcal{I} \subset [\ell], \omega \in [0, 2\pi]} |\mathcal{I}| \\ \text{s.t.} \quad & \|\mathbf{y}_i - \mathbf{R}\mathbf{x}_i\|_2 \leq c, \quad \forall i \in \mathcal{I} \\ & \mathbf{R} = \mathbf{b}\mathbf{b}^\top + [\mathbf{b}]_\times \sin(\omega) + (\mathbf{I}_3 - \mathbf{b}\mathbf{b}^\top) \cos(\omega) \end{aligned} \quad (7)$$

Here $[\mathbf{b}]_\times \in \mathbb{R}^{3 \times 3}$ denotes the matrix generating the cross product \times by \mathbf{b} , that is $[\mathbf{b}]_\times \mathbf{a} = \mathbf{b} \times \mathbf{a}$ for all $\mathbf{a} \in \mathbb{R}^3$. Similarly to Proposition 2, we have the following result:

Proposition 3. *Problem (7) can be solved in $O(\ell \log \ell)$ time and $O(\ell)$ space via interval stabbing.*

After solving (7) with $\mathbf{b} = \mathbf{b}_j$ for each $j \in [s]$, we obtain s candidate consensus sets $\tilde{\mathcal{I}}_1, \dots, \tilde{\mathcal{I}}_s$, and we choose the one with maximal cardinality as an approximate solution to (4). Finally, notice that the time complexity $O(s\ell \log \ell)$ of ARCS+_o depends on the hyper-parameter s . We set $s = 90$ as an invariant choice, as suggested by Figure 1.

This output consensus set $\tilde{\mathcal{I}}$ typically has very few outliers; see Table 3. Thus it will be used next in ARCS+_R, our final step for accurately estimating the rotation (§4.3).

Table 3. The output of ARCS+_o with inputs from Table 2.

Input Inlier Ratio	200 36622	1000 931208	2000 3762888
Output Inlier Ratio	199 213	993 1314	1951 3184

4.3. Step 3: Rotation Estimation

The final step ARCS+_R of ARCS+ is a refinement procedure that performs robust rotation search on the output correspondences $\tilde{\mathcal{I}}$ of ARCS+_o. Since $\tilde{\mathcal{I}}$ contains much fewer

outlier correspondences than we previously had (cf. Table 2 and 3), in what follows we simplify the notations by focusing on the point set $\{(\mathbf{y}_i, \mathbf{x}_i)\}_{i \in [\ell]}$, which we assume has few outliers (say $\leq 50\%$). Then, a natural formulation is

$$\min_{\mathbf{R} \in \text{SO}(3)} \sum_{i=1}^{\ell} \|\mathbf{y}_i - \mathbf{R}\mathbf{x}_i\|_2. \quad (8)$$

Problem (8) appears easier to solve than consensus maximization (4), as it has a convex objective function at least. Next we present the ARCS_{+R} algorithm and its theory.

Algorithm. We start with the following equivalence.

Proposition 4. We have $\mathbf{w}^\top \mathbf{D}_i \mathbf{w} = \|\mathbf{y}_i - \mathbf{R}\mathbf{x}_i\|_2^2$, where $\mathbf{w} \in \mathbb{S}^3$ is a quaternion representation of \mathbf{R} of (8), and $\mathbf{D}_i \in \mathbb{R}^{4 \times 4}$ is a positive semi-definite matrix whose entries depend on $\mathbf{x}_i, \mathbf{y}_i$. So Problem (8) is equivalent to

$$\min_{\mathbf{w} \in \mathbb{S}^3} h(\mathbf{w}), \quad h(\mathbf{w}) = \sum_{i=1}^{\ell} \sqrt{\mathbf{w}^\top \mathbf{D}_i \mathbf{w}}. \quad (9)$$

The exact relation between unit quaternions and rotations is reviewed in Appendix A, where Proposition 4 is proved and the expression of \mathbf{D}_i is given. For what follows, it suffices to know that a unit quaternion is simply a unit vector of \mathbb{R}^4 , and that the space of unit quaternions is \mathbb{S}^3 .

Note that the objective h of (9) is convex, while both problems (8) and (9) are nonconvex (due to the constraint) and nonsmooth (due to the objective). Though (8) and (9) are equivalent, the advantage of (9) will manifest itself soon. Before that, we first introduce the ARCS_{+R} algorithm for solving (9). ARCS_{+R} falls into the general Riemannian subgradient descent framework (see, e.g., [60]). It is initialized at some unit quaternion $\mathbf{w}^{(0)} \in \mathbb{S}^3$ and proceeds by

$$\mathbf{w}^{(t+1)} \leftarrow \text{Proj}_{\mathbb{S}^3}(\mathbf{w}^{(t)} - \gamma^{(t)} \tilde{\nabla}_s h(\mathbf{w}^{(t)})), \quad (10)$$

where $\text{Proj}_{\mathbb{S}^3}(\cdot)$ projects a vector onto \mathbb{S}^3 , $\gamma^{(t)}$ is some step-size, $\tilde{\nabla}_s h(\mathbf{w}^{(t)})$ is a Riemannian subgradient⁵ of h at $\mathbf{w}^{(t)}$.

Theory. Now we are able to compare (8) and (9) from a theoretical perspective. As proved in [16], for any fixed outlier ratio and $k^* > 0$, Riemannian subgradient descent when applied to (8) with proper initialization converges to \mathbf{R}^* in finite time, as long as i) ℓ is sufficiently large, ii) all points \mathbf{y}_i 's and \mathbf{x}_i 's are uniformly distributed on \mathbb{S}^2 , iii) there is no noise. But in [16] no convergence rate is given. One main challenge of establishing convergence rates there is that projecting on $\text{SO}(3)$ does not enjoy a certain kind of *nonexpansiveness* property, which is important for convergence analysis (cf. Lemma 1 of [60]). On the other hand,

⁵We follow [60] where a Riemannian subgradient $\tilde{\nabla}_s h(\mathbf{w})$ at $\mathbf{w} \in \mathbb{S}^3$ is defined as the projection of some subgradient $\nabla_s h(\mathbf{w})$ of h at \mathbf{w} onto the tangent space of \mathbb{S}^3 at \mathbf{w} , i.e., $\tilde{\nabla}_s h(\mathbf{w}) := (\mathbf{I}_4 - \mathbf{w}\mathbf{w}^\top) \nabla_s h(\mathbf{w})$. See [12] for how to compute a subgradient of some given function.

projection onto \mathbb{S}^3 of (9) does satisfy such property. As a result, we are able to provide convergence rate guarantees for ARCS_{+R}. For example, it follows directly from Theorem 2 of [60] that ARCS_{+R} (10) converges to an ε -stationary point in $O(\varepsilon^{-4})$ iterations, even if initialized arbitrarily.

We next give conditions for ARCS_{+R} to converge linearly to the ground-truth unit quaternion $\pm \mathbf{w}^*$ that represents \mathbf{R}^* . Let the distance between a unit quaternion \mathbf{w} and $\pm \mathbf{w}^*$ be

$$\text{dist}(\mathbf{w}, \pm \mathbf{w}^*) := \min \{ \|\mathbf{w} - \mathbf{w}^*\|_2, \|\mathbf{w} + \mathbf{w}^*\|_2 \}.$$

If $\text{dist}(\mathbf{w}, \pm \mathbf{w}^*) < \rho$ with $\rho > 0$ then \mathbf{w} is called ρ -close to $\pm \mathbf{w}^*$. We need the following notion of *sharpness*.

Definition 1 (sharpness [18, 50, 56, 60]). We say that $\pm \mathbf{w}^*$ is an α -sharp minimum of (9) if $\alpha > 0$ and if there exists a number $\rho_\alpha > 0$ such that any unit quaternion $\mathbf{w} \in \mathbb{S}^3$ that is ρ_α -close to $\pm \mathbf{w}^*$ satisfies the inequality

$$h(\mathbf{w}) - h(\mathbf{w}^*) \geq \alpha \text{dist}(\mathbf{w}, \pm \mathbf{w}^*). \quad (11)$$

We provide a condition below for $\pm \mathbf{w}^*$ to be α^* -sharp:

Proposition 5. If $\alpha^* := k^* \eta_{\min} / \sqrt{2} - (\ell - k^*) \eta_{\max} > 0$ and if $\varepsilon_i = \mathbf{0}$ in Problem 2, then Problem (9) admits $\pm \mathbf{w}^*$ as an α^* -sharp minimum. Here η_{\min}, η_{\max} are respectively

$$\eta_{\min} := \frac{1}{k^*} \min_{\mathbf{w} \in \mathcal{S}^* \cap \mathbb{S}^3} \sum_{i \in \mathcal{I}^*} \sqrt{\mathbf{w}^\top \mathbf{D}_i \mathbf{w}}, \quad \text{and} \quad (12)$$

$$\eta_{\max} := \frac{1}{\ell - k^*} \max_{\mathbf{w} \in \mathbb{S}^3} \sum_{i \in [\ell] \setminus \mathcal{I}^*} \sqrt{\mathbf{w}^\top \mathbf{D}_i \mathbf{w}}, \quad (13)$$

where \mathcal{S}^* is the hyperplane of \mathbb{R}^4 perpendicular to $\pm \mathbf{w}^*$.

Proposition 5 is proved in Appendix B.1. The condition $\alpha^* > 0$ defines a relation between the number of inliers (k^*) and outliers ($\ell - k^*$), and involves two quantities η_{\min} and η_{\max} whose values depend on how \mathbf{D}_i 's are distributed on the positive semi-definite cone. We offer probabilistic interpretations for η_{\min} and η_{\max} in Appendix B.2.

With Theorem 4 of [60] and Proposition 5 we have that ARCS_{+R} (10), if initialized properly and with suitable step-sizes, converges linearly to the ground-truth unit quaternion $\pm \mathbf{w}^*$, as long as $\pm \mathbf{w}^*$ is α^* -sharp. A formal statement is:

Theorem 2. Suppose $\alpha^* := k^* \eta_{\min} / \sqrt{2} - (\ell - k^*) \eta_{\max} > 0$. Let L_h be a Lipschitz constant of h . Run Riemannian subgradient descent ARCS_{+R} (10) with initialization $\mathbf{w}^{(0)}$ satisfying $\text{dist}(\mathbf{w}^{(0)}, \pm \mathbf{w}^*) \leq \min\{\alpha^* / L_h, \rho_{\alpha^*}\}$ and with geometrically diminishing stepsizes $\gamma^{(t)} = \beta^t \gamma^{(0)}$, where

$$\gamma^{(0)} < \min \left\{ \frac{2e_0(\alpha^* - L_h e_0)}{L_h^2}, \frac{e_0}{2(\alpha^* - L_h e_0)} \right\},$$

$$\beta^2 \in \left[1 + 2 \left(L_h - \frac{\alpha^*}{e_0} \right) \gamma^{(0)} + \frac{L_h^2 (\gamma^{(0)})^2}{e_0^2}, 1 \right),$$

$$e_0 = \min \left\{ \max \left\{ \text{dist}(\mathbf{w}^{(0)}, \pm \mathbf{w}^*), \frac{\alpha^*}{2L_h} \right\}, \rho_{\alpha^*} \right\}.$$

Table 4. Average errors in degrees | standard deviation | running times in seconds of various algorithms on synthetic data (20 trials).

Inlier Ratio $\frac{k^*}{\ell}$	$\frac{10^3}{10^5} = 1\%$	$\frac{10^3}{10^6} = 0.1\%$	$\frac{3 \times 10^3}{5 \times 10^6} = 0.06\%$	$\frac{3 \times 10^3}{10^7} = 0.03\%$	$\frac{10^3}{10^7} = 0.01\%$
TEASER++ [91]	out-of-memory				
RANSAC	0.39 0.20 29.1	≥ 8.4 hours			
GORE [19, 72]	3.43 2.10 1698	≥ 12 hours			
FGR [96]	52.2 68.5 3.64	95.0 60.9 37.7	84.9 59.4 145	86.5 56.9 311	97.3 61.3 314
GNC-TLS [87]	3.86 9.51 0.13	63.4 50.5 2.26	49.9 31.1 15.9	90.2 45.6 40.1	120 34.3 36.3
ARCS+ _R	9.92 13.1 0.12	65.2 48.9 0.96	55.6 38.3 5.58	88.4 36.2 12.6	98.2 36.0 12.2
ARCS+ _O	0.86 0.29 1.71	0.99 0.37 23.2	0.91 0.30 125	0.98 0.42 287	55.6 60.9 281
ARCS+ _{OR}	0.03 0.03 1.72	0.09 0.07 23.2	0.11 0.07 125	0.22 0.15 287	55.4 60.1 281

In the noiseless case ($\epsilon_i = 0$) we have each $\mathbf{w}^{(t)}$ satisfying

$$\text{dist}(\mathbf{w}^{(t)}, \pm \mathbf{w}^*) \leq \beta^t e_0. \quad (14)$$

Remark 3 (a posteriori optimality guarantees). Theorem 2 endows ARCS+_R (10) with convergence guarantee. On the other hand, a *a posteriori* optimality guarantees can be obtained via semidefinite certification [6, 22, 89, 91].

5. Experiments

In this section we evaluate ARCS+ via synthetic and real experiments for Problem 1, simultaneous rotation and correspondence search. We also evaluate its components, namely ARCS+_O (§4.2) and ARCS+_R (§4.3) for Problem 2, robust rotation search, as it is a task of independent interest. For both of the two problems we compare the following state-of-the-art methods (reviewed in §2): FGR [96], GORE [19], RANSAC, GNC-TLS [87], and TEASER++ [91].

5.1. Experiments on Synthetic Point Clouds

Setup. We set $\sigma = 0.01$, $\bar{c} = c = 5.54\sigma$, $n = \lfloor 0.8m \rfloor$, and $s = 90$ unless otherwise specified. For all other methods we used default or otherwise appropriate parameters. We implemented ARCS+ in MATLAB. No parallelization was explicitly used and no special care was taken for speed.

Robust Rotation Search. From $\mathcal{N}(0, \mathbf{I}_3)$ we randomly sampled point pairs $\{(\mathbf{y}_i, \mathbf{x}_i)\}_{i=1}^\ell$ with k^* inliers and noise $\epsilon_i \sim \mathcal{N}(0, \sigma^2 \mathbf{I}_3)$. Specifically, we generated the ground-truth rotation \mathbf{R}^* from an axis randomly sampled from \mathbb{S}^2 and an angle from $[0, 2\pi]$, rotated k^* points randomly sampled from $\mathcal{N}(0, \mathbf{I}_3)$ by \mathbf{R}^* , and added noise to obtain k^* inlier pairs. Every outlier point \mathbf{y}_j or \mathbf{x}_j was randomly sampled from $\mathcal{N}(0, \mathbf{I}_3)$ with the constraint $-c \leq \|\mathbf{y}_j\|_2 - \|\mathbf{x}_j\|_2 \leq c$; otherwise $(\mathbf{y}_j, \mathbf{x}_j)$ might simply be detected and removed by computing $\|\mathbf{y}_j\|_2 - \|\mathbf{x}_j\|_2$.

We compared ARCS+_O and ARCS+_R and their combination ARCS+_{OR} with prior works. The results are in Table 4. We first numerically illustrate the *accuracy versus scalability* dilemma in prior works (§2). On the one

hand, we observed an extreme where *accuracy overcomes scalability*: RANSAC performed well with error 0.39 when $k^*/\ell = 10^3/10^5$, but its running time increased greatly with decreasing inlier ratio, from 29 seconds to more than 8.4 hours. The other extreme is where *scalability overcomes accuracy*: Both GNC-TLS and FGR failed in presence of such many outliers—as expected—even though their running time scales linearly with ℓ .

Table 4 also depicted the performance of our proposals ARCS+_O and ARCS+_R. Our approximate consensus strategy ARCS+_O reached a balance between accuracy and scalability. In terms of accuracy, it made errors smaller than 1 degree, as long as there are more than $3 \times 10^3/10^7 = 0.03\%$ inliers; this was further refined by Riemannian subgradient descent ARCS+_R, so that their combination ARCS+_{OR} had even lower errors. In terms of scalability, we observed that ARCS+_{OR} is uniformly faster than FGR, and is at least 1800 times faster than GORE for $k^*/\ell = 10^3/10^6 = 0.1\%$. But it had been harder to measure exactly how faster ARCS+_{OR} is than GORE and RANSAC for even larger point sets. Finally, ARCS+_{OR} failed at $k^*/\ell = 10^3/10^7 = 0.01\%$.

Simultaneous Rotation and Correspondence Search. We randomly sampled point sets \mathcal{Q} and \mathcal{P} from $\mathcal{N}(0, \mathbf{I}_3)$ with k^* inlier pairs and noise $\epsilon_{i,j} \sim \mathcal{N}(0, \sigma^2 \mathbf{I}_3)$ (cf. Problem 1). Each outlier point was randomly and independently drawn also from $\mathcal{N}(0, \mathbf{I}_3)$. Figure 2 shows that ARCS+ accurately estimated the rotations for $k^* \geq 2000$ (in 90 seconds), and broke down at $k^* = 1000$, a situation where there were $k^*/m = 10\%$ overlapping points. We did not compare methods like TEASER++, GORE, RANSAC here, because giving them correspondences from ARCS+_N would result unsatisfactory running time or accuracy (recall Tables 2 and 4), while feature matching methods like FPFH do not perform well on random synthetic data.

5.2. Experiments on 3DMatch

The 3DMatch⁶ dataset [95] contains more than 1000 point clouds for testing, representing 8 different scenes

⁶License info: <https://3dmatch.cs.princeton.edu/>

Table 5. Success rates of methods run on the scene pairs of the 3DMatch dataset [95] for which the ground-truth rotation and translation are provided (rotation error smaller than 10 degree means a success [91]; see also the first paragraph of Appendix E).

Scene Type	Kitchen	Home 1	Home 2	Hotel 1	Hotel 2	Hotel 3	Study Room	MIT Lab	Overall
# Scene Pairs	506	156	208	226	104	54	292	77	1623
TEASER++	99.0%	98.1%	94.7%	98.7%	99.0%	98.1%	97.0%	94.8%	97.72%
ARCS++ _{OR}	98.4%	97.4%	95.7%	98.7%	98.1%	100%	97.3%	96.1%	97.72%

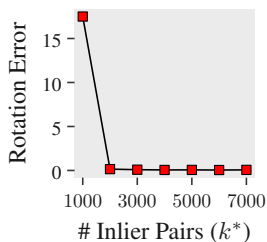


Figure 2. Rotation errors of ARCS+ on synthetic Gaussian point clouds. 20 trials, $m = 10^4$, $n = \lceil 0.8m \rceil$, $\sigma = 0.01$.

(such as kitchen, hotel, etc.), while the number of point clouds for each scene ranges from 77 to 506. Each point cloud has more than 10^5 points, yet in [95] there are 5000 keypoints for each cloud. We used the pretrained model⁷ of the 3DSmoothNet [35] to extract descriptors from these key points, and matched them using the Matlab function `pcmatchfeatures`, with its parameter `MatchThreshold` set to the maximum 1. We assume that the ground-truth translation \mathbf{t}^* is given, and run TEASER++ and ARCS+_{OR} on $(\mathbf{y}_i - \mathbf{t}^*, \mathbf{x}_i)$'s; the performance is comparable. We did not compare other methods here, as TEASER++ currently has the best performance on 3DMatch (to the best of our knowledge); see [91] for comparison with optimization-based methods, and see [25] for the success rates (recall) of deep learning methods.

See the supplementary materials for more experiments.

6. Discussion and Future Work

Despite of the progress that we made for robust rotation search and simultaneous rotation and correspondence search on large-scale point clouds, our ARCS+ pipeline has a few limitations, and we discuss them next.

For small datasets (e.g., $\ell \leq 500$), as in homography fitting [19], other methods, e.g., MAGSAC++ [7–9], VSAC [45], TEASER++ [91], and GORE [19] might be considered with higher priority; they come with efficient C++ implementations. For more points, e.g., $\ell \geq 10^4$, but with higher inlier rates than in Table 4 (e.g., $\geq 15\%$), GNC-TLS [87] and RANSAC are our recommendations for what to use.

⁷<https://github.com/zgojcic/3DSmoothNet>

Modern point clouds have more than 10^5 points, and are naturally correspondences-less (cf. [20]). ARCS operates at that scale in the absence of noise (Table 1), while ARCS+ can handle $m, n \approx 10000$ (Figure 2) and ARCS+_{OR} can handle $\ell \approx 10^7$ correspondences (Table 4); all these are limited to the rotation-only case. To find rotation (and translation) from such point sets “in the wild”, it seems inevitable to downsample them. An interesting future work is to theoretically quantify the tradeoff between downsampling factors and the final registration performance. Another tradeoff to quantify, as implied by Remark 2, is this: Can we design a correspondence matching algorithm that better balances the number of remaining points and the number of remaining inliers? In particular, such matching should take specific pose into consideration (cf. ARCS); many methods did not.

Like TEASER++, GORE, GNC-TLS, RANSAC, our algorithm relies on an inlier threshold c . While how to set this hyper-parameter suitably is known for Gaussian noise with given variance, *in practice the distance threshold is usually chosen empirically*, as Hartley & Zisserman wrote [38]. While mis-specification of c could fail the registration, certain heuristics have been developed to alleviate the sensitivity to such mis-specification; see [3, 7–9]. Finally, our experience is to set c based on the scale of the point clouds.

Our outlier removal component ARCS+_O presented good performance (Table 3), yet with no optimality guarantees. Note that, with $s = 90$ we have $|\phi_j - \phi^*| \leq 1$ for some ϕ_j , while Figure 1a shows that ARCS+_O gave roughly 1 degree error at $s = 90$. Theoretically justifying this is left as future work. Without guarantees, registration could fail, which might lead to undesired consequences in safety-critical applications. On the other hand, we believe that ARCS+ is a good demonstration of trading optimality guarantees for accuracy and scalability; enforcing all of the three properties amounts to requiring solving NP hard problems efficiently at large scale! In fact, since any solutions might get certified for optimality (Remark 3), bold algorithmic design ideas can be taken towards improving accuracy and scalability, while relying on other tools for optimality certification.

Acknowledgments. The first author was supported by the MINDS PhD fellowship at Johns Hopkins University. This work was supported by NSF Grants 1704458 and 1934979, and by the Northrop Grumman Mission Systems Research in Applications for Learning Machines (REALM) initiative.

References

- [1] Simon L Altmann. Hamilton, Rodrigues, and the quaternion scandal. *Mathematics Magazine*, 62(5):291–308, 1989. [12](#)
- [2] Pasquale Antonante, Vasileios Tzoumas, Heng Yang, and Luca Carlone. Outlier-robust estimation: Hardness, minimally-tuned algorithms, and applications. Technical report, arXiv:2007.15109v2 [cs.CV], 2020. [1](#)
- [3] Pasquale Antonante, Vasileios Tzoumas, Heng Yang, and Luca Carlone. Outlier-robust estimation: Hardness, minimally tuned algorithms, and applications. *IEEE Transactions on Robotics*, 2021. [8](#)
- [4] K Somani Arun, Thomas S Huang, and Steven D Blostein. Least-squares fitting of two 3D point sets. *IEEE Transactions on Pattern Analysis and Machine Intelligence*, (5):698–700, 1987. [3](#)
- [5] Xuyang Bai, Zixin Luo, Lei Zhou, Hongkai Chen, Lei Li, Zeyu Hu, Hongbo Fu, and Chiew-Lan Tai. Pointdsc: Robust point cloud registration using deep spatial consistency. In *IEEE Conference on Computer Vision and Pattern Recognition*, pages 15859–15869, 2021. [1](#)
- [6] Afonso S Bandeira. A note on probably certifiably correct algorithms. *Comptes Rendus Mathématique*, 354(3):329–333, 2016. [7](#)
- [7] Daniel Barath, Jiri Matas, and Jana Noskova. Magsac: marginalizing sample consensus. In *IEEE/CVF Conference on Computer Vision and Pattern Recognition*, pages 10197–10205, 2019. [8](#), [16](#)
- [8] Daniel Barath, Jana Noskova, Maksym Ivashechkin, and Jiri Matas. Magsac++, a fast, reliable and accurate robust estimator. In *IEEE/CVF conference on computer vision and pattern recognition*, pages 1304–1312, 2020. [8](#), [16](#)
- [9] Daniel Barath, Jana Noskova, and Jiri Matas. Marginalizing sample consensus. *IEEE Transactions on Pattern Analysis and Machine Intelligence*, 2021. [8](#), [16](#)
- [10] Dominik Bauer, Timothy Patten, and Markus Vincze. Reagent: Point cloud registration using imitation and reinforcement learning. In *IEEE Conference on Computer Vision and Pattern Recognition*, pages 14586–14594, 2021. [1](#)
- [11] Jean-Charles Bazin, Yongduek Seo, and Marc Pollefeys. Globally optimal consensus set maximization through rotation search. In *Asian Conference on Computer Vision*, pages 539–551, 2012. [2](#)
- [12] Amir Beck. *First-Order Methods in Optimization*. Society for Industrial and Applied Mathematics, 2017. [6](#)
- [13] Amir Beck, Petre Stoica, and Jian Li. Exact and approximate solutions of source localization problems. *IEEE Transactions on signal processing*, 56(5):1770–1778, 2008. [19](#)
- [14] Lukas Bernreiter, Lionel Ott, Juan Nieto, Roland Siegwart, and Cesar Cadena. PHASER: A robust and correspondence-free global pointcloud registration. *IEEE Robotics and Automation Letters*, 6(2):855–862, 2021. [1](#)
- [15] PJ Besl and Neil D McKay. A method for registration of 3D shapes. *IEEE Transactions on Pattern Analysis and Machine Intelligence*, 14(2):239–256, 1992. [1](#), [2](#)
- [16] Cindy Orozco Bohorquez, Yuehaw Khoo, and Lexing Ying. Maximizing robustness of point-set registration by leveraging non-convexity. Technical report, arXiv:2004.08772v3 [math.OC], 2020. [2](#), [6](#), [17](#)
- [17] Stéphane Boucheron, Gábor Lugosi, and Pascal Massart. *Concentration inequalities: A nonasymptotic theory of independence*. Oxford university press, 2013. [15](#)
- [18] James V Burke and Michael C Ferris. Weak sharp minima in mathematical programming. *SIAM Journal on Control and Optimization*, 31(5):1340–1359, 1993. [6](#)
- [19] Álvaro Parra Bustos and Tat-Jun Chin. Guaranteed outlier removal for rotation search. In *IEEE International Conference on Computer Vision*, pages 2165–2173, 2015. [1](#), [2](#), [4](#), [5](#), [7](#), [8](#), [16](#)
- [20] Zhipeng Cai, Tat-Jun Chin, Alvaro Parra Bustos, and Konrad Schindler. Practical optimal registration of terrestrial lidar scan pairs. *ISPRS Journal of Photogrammetry and Remote Sensing*, 147:118–131, 2019. [4](#), [8](#)
- [21] Dylan Campbell and Lars Petersson. GOGMA: Globally-optimal gaussian mixture alignment. In *IEEE Conference on Computer Vision and Pattern Recognition*, 2016. [1](#), [2](#)
- [22] Luca Carlone, Giuseppe C. Calafiore, Carlo Tommolillo, and Frank Dellaert. Planar pose graph optimization: Duality, optimal solutions, and verification. *IEEE Transactions on Robotics*, 32(3):545–565, 2016. [7](#)
- [23] Dmitry Chetverikov, Dmitry Svirko, Dmitry Stepanov, and Pavel Krsek. The trimmed iterative closest point algorithm. In *Object recognition supported by user interaction for service robots*, volume 3, pages 545–548, 2002. [1](#), [2](#)
- [24] Tat-Jun Chin, Yang Heng Kee, Anders Eriksson, and Frank Neumann. Guaranteed outlier removal with mixed integer linear programs. In *IEEE Conference on Computer Vision and Pattern Recognition*, pages 5858–5866, 2016. [1](#)
- [25] Christopher Choy, Wei Dong, and Vladlen Koltun. Deep global registration. In *IEEE Conference on Computer Vision and Pattern Recognition*, 2020. [1](#), [8](#), [16](#), [20](#)
- [26] Haili Chui and Anand Rangarajan. A new point matching algorithm for non-rigid registration. *Computer Vision and Image Understanding*, 89(2-3):114–141, 2003. [1](#), [2](#)
- [27] Brian Curless and Marc Levoy. A volumetric method for building complex models from range images. In *Annual Conference on Computer Graphics and Interactive Techniques*, pages 303–312, 1996. [18](#)
- [28] Mark De Berg, Marc Van Kreveld, Mark Overmars, and Otfried Schwarzkopf. *Computational Geometry*. Springer, 1997. [2](#), [4](#)
- [29] Tianjiao Ding, Yunchen Yang, Zhihui Zhu, Daniel P Robinson, René Vidal, Laurent Kneip, and Manolis C Tsakiris. Robust homography estimation via dual principal component pursuit. In *IEEE Conference on Computer Vision and Pattern Recognition*, pages 6080–6089, 2020. [13](#)
- [30] Tianyu Ding, Zhihui Zhu, Tianjiao Ding, Yunchen Yang, René Vidal, Manolis C. Tsakiris, and Daniel Robinson. Noisy dual principal component pursuit. In *International Conference on Machine Learning*, pages 1617–1625, 2019. [5](#), [13](#)
- [31] Tianyu Ding, Zhihui Zhu, René Vidal, and Daniel P Robinson. Dual principal component pursuit for robust subspace learning: Theory and algorithms for a holistic approach.

- In *International Conference on Machine Learning*, pages 2739–2748, 2021. 5
- [32] Richard Everson. Orthogonal, but not orthonormal, Procrustes problems. *Advances in Computational Mathematics*, 3(4), 1998. 1
- [33] Martin A Fischler and Robert C Bolles. Random sample consensus: a paradigm for model fitting with applications to image analysis and automated cartography. *Communications of the ACM*, 24(6):381–395, 1981. 1
- [34] Xiao-Shan Gao, Xiao-Rong Hou, Jianliang Tang, and Hang-Fei Cheng. Complete solution classification for the perspective-three-point problem. *IEEE Transactions on Pattern Analysis and Machine Intelligence*, 25(8):930–943, 2003. 2
- [35] Zan Gojcic, Caifa Zhou, Jan D. Wegner, and Andreas Wieser. The perfect match: 3D point cloud matching with smoothed densities. In *IEEE Conference on Computer Vision and Pattern Recognition*, pages 5540–5549, 2019. 2, 8, 20
- [36] John C Gower, Garnt B Dijkstra, et al. *Procrustes Problems*, volume 30. Oxford University Press on Demand, 2004. 1
- [37] Eric N. Hanson. The interval skip list: A data structure for finding all intervals that overlap a point. In *Algorithms and Data Structures*, pages 153–164, 1991. 4
- [38] Richard Hartley and Andrew Zisserman. *Multiple View Geometry in Computer Vision*. Cambridge University Press, 2004. 8
- [39] Richard I Hartley and Fredrik Kahl. Global optimization through rotation space search. *International Journal of Computer Vision*, 82(1):64–79, 2009. 1, 2
- [40] Berthold KP Horn. Closed-form solution of absolute orientation using unit quaternions. *Journal of the Optical Society of America A*, 4(4):629–642, 1987. 3
- [41] Berthold KP Horn, Hugh M Hilden, and Shahriar Negahdaripour. Closed-form solution of absolute orientation using orthonormal matrices. *Journal of the Optical Society of America A*, 5(7):1127–1135, 1988. 3
- [42] Shengyu Huang, Zan Gojcic, Mikhail Usvatsov, Andreas Wieser, and Konrad Schindler. PREDATOR: Registration of 3D point clouds with low overlap. In *IEEE Conference on Computer Vision and Pattern Recognition*, pages 4267–4276, 2021. 1
- [43] Xiaoshui Huang, Guofeng Mei, Jian Zhang, and Rana Abbas. A comprehensive survey on point cloud registration. Technical report, arXiv:2103.02690v2 [cs.CV], 2021. 1
- [44] Jose Pedro Iglesias, Carl Olsson, and Fredrik Kahl. Global optimality for point set registration using semidefinite programming. In *IEEE Conference on Computer Vision and Pattern Recognition*, 2020. 1
- [45] Maksym Ivashechkin, Daniel Barath, and Jiří Matas. Vsac: Efficient and accurate estimator for h and f. In *IEEE/CVF International Conference on Computer Vision*, pages 15243–15252, 2021. 8, 16
- [46] Bing Jian and Baba C. Vemuri. Robust point set registration using gaussian mixture models. *IEEE Transactions on Pattern Analysis and Machine Intelligence*, 33(8):1633–1645, 2011. 1, 2
- [47] Yanmei Jiao, Yue Wang, Bo Fu, Qimeng Tan, Lei Chen, Minghang Wang, Shoudong Huang, and Rong Xiong. Globally optimal consensus maximization for robust visual inertial localization in point and line map. In *International Conference on Intelligent Robots and Systems*, pages 4631–4638, 2020. 5
- [48] Kyungdon Joo, Hongdong Li, Tae-Hyun Oh, and In So Kweon. Robust and efficient estimation of relative pose for cameras on selfie sticks. *IEEE Transactions on Pattern Analysis and Machine Intelligence*, 2021. 2
- [49] Sham Kakade. Symmetrization and Rademacher averages. Technical report, Lecture 11 of Stat 928: Statistical Learning Theory, 2011. 15
- [50] Mohammad Mahdi Karkhaneei and Nezam Mahdavi-Amiri. Nonconvex weak sharp minima on Riemannian manifolds. *Journal of Optimization Theory and Applications*, 183(1):85–104, 2019. 6
- [51] Zuzana Kukelova, Martin Bujnak, and Tomas Pajdla. Automatic generator of minimal problem solvers. In *European Conference on Computer Vision*, pages 302–315, 2008. 2
- [52] Viktor Larsson, Kalle Astrom, and Magnus Oskarsson. Efficient solvers for minimal problems by syzygy-based reduction. In *IEEE Conference on Computer Vision and Pattern Recognition*, pages 2383–2392, 2017. 2
- [53] Viktor Larsson, Magnus Oskarsson, Kalle Astrom, Alge Wallis, Zuzana Kukelova, and Tomas Pajdla. Beyond grobner bases: Basis selection for minimal solvers. In *IEEE Conference on Computer Vision and Pattern Recognition*, 2018. 2
- [54] Gilad Lerman and Tyler Maunu. An overview of robust subspace recovery. *Proceedings of the IEEE*, 106(8):1380–1410, 2018. 5
- [55] Gilad Lerman, Michael B. McCoy, Joel A. Tropp, and Teng Zhang. Robust computation of linear models by convex relaxation. *Foundations of Computational Mathematics*, 15(2):363–410, 2015. 14
- [56] Chong Li, Boris S. Mordukhovich, Jinhua Wang, and Jen-Chih Yao. Weak sharp minima on Riemannian manifolds. *SIAM Journal on Optimization*, 21(4):1523–1560, 2011. 6
- [57] Hongdong Li and Richard Hartley. The 3D-3D registration problem revisited. In *IEEE International Conference on Computer Vision*, pages 1–8, 2007. 1, 2
- [58] Jiayuan Li, Qingwu Hu, and Mingyao Ai. GESAC: Robust graph enhanced sample consensus for point cloud registration. *ISPRS Journal of Photogrammetry and Remote Sensing*, 167:363–374, 2020. 1, 2
- [59] Jiayuan Li, Qingwu Hu, and Mingyao Ai. Point cloud registration based on one-point RANSAC and scale-annealing biweight estimation. *IEEE Transactions on Geoscience and Remote Sensing*, pages 1–14, 2021. 1
- [60] Xiao Li, Shixiang Chen, Zengde Deng, Qing Qu, Zhihui Zhu, and Anthony Man-Cho So. Weakly convex optimization over Stiefel manifold using Riemannian subgradient-type methods. *SIAM Journal on Optimization*, 31(3):1605–1634, 2021. 2, 6, 13, 14
- [61] Wei Lian, Lei Zhang, and Ming-Hsuan Yang. An efficient globally optimal algorithm for asymmetric point matching.

- IEEE Transactions on Pattern Analysis and Machine Intelligence*, 39(7):1281–1293, 2017. 1
- [62] Yinlong Liu, Chen Wang, Zhijian Song, and Manning Wang. Efficient global point cloud registration by matching rotation invariant features through translation search. In *European Conference on Computer Vision*, 2018. 1, 2, 19
- [63] Parker C. Lusk, Kaveh Fathian, and Jonathan P. How. CLIPPER: A graph-theoretic framework for robust data association. Technical report, arXiv:2011.10202v2 [cs.RO], 2021. 2
- [64] F Landis Markley. Attitude determination using vector observations and the singular value decomposition. *Journal of the Astronautical Sciences*, 36(3):245–258, 1988. 3
- [65] Haggai Maron, Nadav Dym, Itay Kezurer, Shahar Kovalsky, and Yaron Lipman. Point registration via efficient convex relaxation. *ACM Transactions on Graphics*, 35(4), 2016. 1
- [66] Andreas Maurer. A vector-contraction inequality for Rademacher complexities. In *International Conference on Algorithmic Learning Theory*, pages 3–17. Springer, 2016. 15
- [67] Colin McDiarmid et al. On the method of bounded differences. *Surveys in Combinatorics*, 141(1):148–188, 1989. 15
- [68] Andriy Myronenko and Xubo Song. Point set registration: Coherent point drift. *IEEE Transactions on Pattern Analysis and Machine Intelligence*, 32(12):2262–2275, 2010. 1, 2
- [69] Yurii Nesterov. *Lectures on Convex Optimization*. Springer, 2018. 5
- [70] David Nistér. An efficient solution to the five-point relative pose problem. *IEEE Transactions on Pattern Analysis and Machine Intelligence*, 26(6):756–770, 2004. 2
- [71] Álvaro Parra, Tat-Jun Chin, Frank Neumann, Tobias Friedrich, and Maximilian Katzmann. A practical maximum clique algorithm for matching with pairwise constraints. Technical report, arXiv:1902.01534v2 [cs.CV], 2020. 1, 2, 19
- [72] Álvaro Parra Bustos and Tat-Jun Chin. Guaranteed outlier removal for point cloud registration with correspondences. *IEEE Transactions on Pattern Analysis and Machine Intelligence*, 40(12):2868–2882, 2018. 1, 2, 4, 7
- [73] Álvaro Parra Bustos, Tat-Jun Chin, Anders Eriksson, Hongdong Li, and David Suter. Fast rotation search with stereographic projections for 3D registration. *IEEE Transactions on Pattern Analysis and Machine Intelligence*, 38(11):2227–2240, 2016. 1, 2
- [74] Mikael Persson and Klas Nordberg. Lambda twist: An accurate fast robust perspective three point (p3p) solver. In *European conference on computer vision*, pages 318–332, 2018. 19
- [75] Ryan A. Rossi, David F. Gleich, and Assefaw H. Gebremedhin. Parallel maximum clique algorithms with applications to network analysis. *SIAM Journal on Scientific Computing*, 37(5):C589–C616, 2015. 2
- [76] Szymon Rusinkiewicz and Marc Levoy. Efficient variants of the ICP algorithm. In *International Conference on 3D Digital Imaging and Modeling*, pages 145–152. IEEE, 2001. 1, 2
- [77] Radu Bogdan Rusu, Nico Blodow, and Michael Beetz. Fast point feature histograms (FPFH) for 3D registration. In *IEEE International Conference on Robotics and Automation*, pages 3212–3217, 2009. 2
- [78] Peter H Schönemann. A generalized solution of the orthogonal Procrustes problem. *Psychometrika*, 31(1):1–10, 1966. 3
- [79] Jingnan Shi, Heng Yang, and Luca Carlone. ROBIN: a graph-theoretic approach to reject outliers in robust estimation using invariants. Technical report, arXiv:2011.03659v2 [cs.CV], 2021. 1, 2, 19
- [80] Julian Straub, Trevor Campbell, Jonathan P How, and John W Fisher. Efficient global point cloud alignment using bayesian nonparametric mixtures. In *IEEE Conference on Computer Vision and Pattern Recognition*, pages 2941–2950, 2017. 1
- [81] Lei Sun. IRON: Invariant-based highly robust point cloud registration. Technical report, arXiv:2103.04357v2 [cs.CV], 2021. 1, 2
- [82] Lei Sun. RANSIC: Fast and highly robust estimation for rotation search and point cloud registration using invariant compatibility. Technical report, arXiv:2104.09133v3 [cs.CV], 2021. 1, 2
- [83] Richard Szeliski. *Computer Vision: Algorithms and Applications*. Springer Science & Business Media, 2010. 16
- [84] Chin Tat-Jun, Cai Zhipeng, and Frank Neumann. Robust fitting in computer vision: Easy or hard? *International Journal of Computer Vision*, 128(3):575–587, 2020. 4
- [85] Manolis C. Tsakiris and René Vidal. Dual principal component pursuit. *Journal of Machine Learning Research*, 19(18):1–50, 2018. 5, 13
- [86] Grace Wahba. A least squares estimate of satellite attitude. *SIAM Review*, 7(3):409, 1965. 1, 3
- [87] Heng Yang, Pasquale Antonante, Vasileios Tzoumas, and Luca Carlone. Graduated non-convexity for robust spatial perception: From non-minimal solvers to global outlier rejection. *IEEE Robotics and Automation Letters*, 5(2):1127–1134, 2020. 1, 3, 7, 8, 17
- [88] Heng Yang and Luca Carlone. A quaternion-based certifiably optimal solution to the Wahba problem with outliers. In *IEEE International Conference on Computer Vision*, pages 1665–1674, 2019. 1, 2, 16
- [89] Heng Yang and Luca Carlone. One ring to rule them all: Certifiably robust geometric perception with outliers. In *Advances in Neural Information Processing Systems*, 2020. 7
- [90] Heng Yang, Ling Liang, Kim-Chuan Toh, and Luca Carlone. STRIDE along spectrahedral vertices for solving large-scale rank-one semidefinite relaxations. Technical report, arXiv:2105.14033 [math.OC], 2021. 1
- [91] Heng Yang, Jingnan Shi, and Luca Carlone. TEASER: Fast and certifiable point cloud registration. *IEEE Transactions on Robotics*, 37(2):314–333, 2021. 1, 2, 3, 7, 8, 16, 18, 19, 20, 21
- [92] Jiaolong Yang, Hongdong Li, Dylan Campbell, and Yunde Jia. Go-ICP: A globally optimal solution to 3D ICP point-set registration. *IEEE Transactions on Pattern Analysis and Machine Intelligence*, 38(11):2241–2254, 2016. 1, 2

- [93] Jiaolong Yang, Hongdong Li, and Yunde Jia. Go-ICP: Solving 3D registration efficiently and globally optimally. In *IEEE International Conference on Computer Vision*, pages 1457–1464, 2013. [2](#)
- [94] Yunzhen Yao, Liangzu Peng, and Manolis Tsakiris. Unlabeled principal component analysis. *Advances in Neural Information Processing Systems*, 2021. [5](#)
- [95] Andy Zeng, Shuran Song, Matthias Nießner, Matthew Fisher, Jianxiong Xiao, and T Funkhouser. 3DMatch: Learning the matching of local 3D geometry in range scans. In *IEEE Conference on Computer Vision and Pattern Recognition*, page 4, 2017. [7](#), [8](#), [19](#), [20](#), [21](#)
- [96] Qian-Yi Zhou, Jaesik Park, and Vladlen Koltun. Fast global registration. In *European Conference on Computer Vision*, pages 766–782, 2016. [1](#), [2](#), [7](#), [17](#)
- [97] Zhihui Zhu, Tianyu Ding, Daniel Robinson, Manolis Tsakiris, and René Vidal. A linearly convergent method for non-smooth non-convex optimization on the grassmannian with applications to robust subspace and dictionary learning. In *Advances in Neural Information Processing Systems*, 2019. [5](#)
- [98] Zhihui Zhu, Yifan Wang, Daniel Robinson, Daniel Naiman, René Vidal, and Manolis C. Tsakiris. Dual principal component pursuit: Improved analysis and efficient algorithms. In *Advances in Neural Information Processing Systems*, 2018. [5](#), [14](#)

A. Proof of Proposition 4

We consider a stronger version of Proposition 4:

Proposition 6. *We have $\mathbf{w}^\top \mathbf{D}_i \mathbf{w} = \|\mathbf{y}_i - \mathbf{R}\mathbf{x}_i\|_2^2$, where \mathbf{w} is a quaternion representation of \mathbf{R} of (8), and $\mathbf{D}_i \in \mathbb{R}^{4 \times 4}$ is a positive semi-definite matrix whose entries depend on $\mathbf{x}_i, \mathbf{y}_i$. So Problem (8) is equivalent to*

$$\min_{\mathbf{w} \in \mathbb{S}^3} h(\mathbf{w}), \quad h(\mathbf{w}) = \sum_{i=1}^{\ell} \sqrt{\mathbf{w}^\top \mathbf{D}_i \mathbf{w}}. \quad (15)$$

Moreover, \mathbf{D}_i has eigenvalues 4, 4, 0, 0 if \mathbf{x}_i and \mathbf{y}_i are normalized (that is $\|\mathbf{x}_i\|_2 = \|\mathbf{y}_i\|_2 = 1$).

We first recall some basics about unit quaternions, an algebraic construction invented by Hamilton in the 1840’s, when the notion of *vector* does not exist; see the beautiful account of [1]. In our current notation, each element \mathbf{w} of \mathbb{S}^3 is called a unit quaternion. The most crucial fact is that $\text{SO}(3)$ is isomorphic to the 3-sphere \mathbb{S}^3 up to sign, that is $\text{SO}(3) \equiv \mathbb{S}^3 / \{\pm 1\}$. This implies a two-to-one correspondence between unit quaternions and 3D rotations. Algebraically, any $\mathbf{R} \in \text{SO}(3)$ can be written as a 3×3 matrix

$$\begin{bmatrix} w_1^2 + w_2^2 - w_3^2 - w_4^2 & 2(w_2w_3 - w_1w_4) & 2(w_2w_4 + w_1w_3) \\ 2(w_2w_3 + w_1w_4) & w_1^2 + w_3^2 - w_2^2 - w_4^2 & 2(w_3w_4 - w_1w_2) \\ 2(w_2w_4 - w_1w_3) & 2(w_3w_4 + w_1w_2) & w_1^2 + w_4^2 - w_2^2 - w_3^2 \end{bmatrix}$$

where $\mathbf{w} = [w_1, w_2, w_3, w_4]^\top \in \mathbb{S}^3$. We can now write the three entries of $\mathbf{R}\mathbf{x}_i$ as quadratic forms $\mathbf{w}^\top \mathbf{X}_{i,1}\mathbf{w}$, $\mathbf{w}^\top \mathbf{X}_{i,2}\mathbf{w}$, and $\mathbf{w}^\top \mathbf{X}_{i,3}\mathbf{w}$, respectively. Here $\mathbf{X}_{i,1}$, $\mathbf{X}_{i,2}$, and $\mathbf{X}_{i,3}$ are 4×4 symmetric matrices, defined as

$$\mathbf{X}_{i,1} = \begin{bmatrix} [\mathbf{x}_i]_1 & 0 & [\mathbf{x}_i]_3 & -[\mathbf{x}_i]_2 \\ 0 & [\mathbf{x}_i]_1 & [\mathbf{x}_i]_2 & [\mathbf{x}_i]_3 \\ [\mathbf{x}_i]_3 & [\mathbf{x}_i]_2 & -[\mathbf{x}_i]_1 & 0 \\ -[\mathbf{x}_i]_2 & [\mathbf{x}_i]_3 & 0 & -[\mathbf{x}_i]_1 \end{bmatrix} \quad (16)$$

$$\mathbf{X}_{i,2} = \begin{bmatrix} [\mathbf{x}_i]_2 & -[\mathbf{x}_i]_3 & 0 & [\mathbf{x}_i]_1 \\ -[\mathbf{x}_i]_3 & -[\mathbf{x}_i]_2 & [\mathbf{x}_i]_1 & 0 \\ 0 & [\mathbf{x}_i]_1 & [\mathbf{x}_i]_2 & [\mathbf{x}_i]_3 \\ [\mathbf{x}_i]_1 & 0 & [\mathbf{x}_i]_3 & -[\mathbf{x}_i]_2 \end{bmatrix} \quad (17)$$

$$\mathbf{X}_{i,3} = \begin{bmatrix} [\mathbf{x}_i]_3 & [\mathbf{x}_i]_2 & -[\mathbf{x}_i]_1 & 0 \\ [\mathbf{x}_i]_2 & -[\mathbf{x}_i]_3 & 0 & [\mathbf{x}_i]_1 \\ -[\mathbf{x}_i]_1 & 0 & -[\mathbf{x}_i]_3 & [\mathbf{x}_i]_2 \\ 0 & [\mathbf{x}_i]_1 & [\mathbf{x}_i]_2 & [\mathbf{x}_i]_3 \end{bmatrix} \quad (18)$$

Defining $\mathbf{C}_i := [\mathbf{y}_i]_1 \mathbf{X}_{i,1} + [\mathbf{y}_i]_2 \mathbf{X}_{i,2} + [\mathbf{y}_i]_3 \mathbf{X}_{i,3}$, we get that $\mathbf{y}_i^\top \mathbf{R}\mathbf{x}_i = \mathbf{w}^\top \mathbf{C}_i \mathbf{w}$. And defining

$$\mathbf{D}_i = (\|\mathbf{y}_i\|_2^2 + \|\mathbf{x}_i\|_2^2) \mathbf{I}_4 - 2\mathbf{C}_i \quad (19)$$

with \mathbf{I}_4 the 4×4 identity matrix, we obtain the equality

$$\|\mathbf{y}_i - \mathbf{R}\mathbf{x}_i\|_2^2 = \|\mathbf{y}_i\|_2^2 + \|\mathbf{x}_i\|_2^2 - 2\mathbf{y}_i^\top \mathbf{R}\mathbf{x}_i \quad (20)$$

$$= \mathbf{w}^\top \mathbf{D}_i \mathbf{w}. \quad (21)$$

Since D_i is symmetric and $\mathbf{w}^\top D_i \mathbf{w} \geq 0$ for any $\mathbf{w} \in \mathbb{S}^3$, we know that $D_i \in \mathbb{R}^{4 \times 4}$ is positive semi-definite.

Suppose $\|\mathbf{y}_i\|_2 = \|\mathbf{x}_i\|_2 = 1$. Then there is at least two different 3D rotations \mathbf{R}_1 and \mathbf{R}_2 satisfying $\mathbf{y}_i = \mathbf{R}_1 \mathbf{x}_i = \mathbf{R}_2 \mathbf{x}_i$. Thus, with the factorization $D_i = \mathbf{Z}_i \mathbf{Z}_i^\top$, there are at least two quaternions \mathbf{w}_1 and \mathbf{w}_2 with $\mathbf{w}_1 \neq \pm \mathbf{w}_2$ satisfying that $\mathbf{Z}_i^\top \mathbf{w}_1 = \mathbf{Z}_i^\top \mathbf{w}_2 = 0$. So $\text{rank}(D_i) = \text{rank}(\mathbf{Z}_i) \leq 2$. Recalling $D_i = 2\mathbf{I}_4 - 2\mathbf{C}_i$, we see that 1 is an eigenvalue of \mathbf{C}_i that has multiplicity at least 2. Similarly, we can derive that $\|\mathbf{y}_i + \mathbf{R}\mathbf{x}_i\|_2^2 = \mathbf{w}^\top D'_i \mathbf{w}$ where $D'_i = (\|\mathbf{y}_i\|_2^2 + \|\mathbf{x}_i\|_2^2)\mathbf{I}_4 + 2\mathbf{C}_i = 2\mathbf{I}_4 + 2\mathbf{C}_i$ is positive semi-definite of rank at most 2. That is, -1 is an eigenvalue of \mathbf{C}_i of multiplicity at least 2. Concluding, \mathbf{C}_i has eigenvalues 1, 1, -1 , -1 and D_i has eigenvalues 4, 4, 0, 0.

B. Proposition 5: Proof and Interpretation

Here we provide a proof (Appendix B.1) and probabilistic interpretation (Appendix B.2) for Proposition 5. In this section, we use the notation $D_i = \mathbf{Z}_i \mathbf{Z}_i^\top$ from Appendix A where we decomposed every positive semidefinite matrix D_i into the product of its root \mathbf{Z}_i . Since we could always normalize the point sets \mathbf{y}_i and \mathbf{x}_i , and then normalize D_i , we assume without loss of generality that D_i has eigenvalues 1, 1, 0, 0 (cf. Proposition 6). In this situation, we can now specify that \mathbf{Z}_i is a matrix of size 4×2 and it has orthonormal columns, i.e., $\mathbf{Z}_i^\top \mathbf{Z}_i = \mathbf{I}_2$. Also, we see that the objective function (9) of interest can be rewritten as

$$\min_{\mathbf{w} \in \mathbb{S}^3} h(\mathbf{w}), \quad h(\mathbf{w}) = \sum_{i=1}^{\ell} \|\mathbf{Z}_i^\top \mathbf{w}\|_2. \quad (22)$$

Note that, if \mathbf{Z}_i had a single column, then (22) is exactly the problem of *dual principal component pursuit* (DPCP) [85]. On the other hand, one could think of (22) as a *group* version of DPCP, as $\|\mathbf{Z}_i^\top \mathbf{w}\|_2$ here promotes group sparsity. A similar group version of DPCP was considered by [29] in the context of homography estimation. In [29], the authors provided conditions under which any global minimizer of (22) coincides with the ground-truth normal vector, or, in our context, the ground-truth unit quaternion $\pm \mathbf{w}^*$. Thus, our contribution here, if viewed from the angle of group-DPCP, is to show that, there is actually an efficient algorithm that exactly reaches the guaranteed ground-truth normal. We present our contribution next.

B.1. Proof of Proposition 5

The proof follows from Proposition 4 of [60] with some simplification for specializing arbitrary Stiefel manifolds to \mathbb{S}^3 , and with some modification to tighten a constant factor (from 2 to $\sqrt{2}$). We also note that η_{\min} and η_{\max} are motivated from their corresponding definitions.

Write $\mathbf{w} := c_0 \mathbf{w}_0 + c^* \mathbf{w}^*$ with $c_0^2 + (c^*)^2 = 1$ and $\mathbf{w}_0 \in \mathcal{S}^*$. Without loss of generality assume $c^* \geq 0$. Then

$$\begin{aligned} \text{dist}(\mathbf{w}, \pm \mathbf{w}^*) &= \min \{ \sqrt{2 + 2c^*}, \sqrt{2 - 2c^*} \} \\ &= \sqrt{2 - 2c^*} \\ &\leq \sqrt{2 - 2(c^*)^2} = \sqrt{2}c_0. \end{aligned} \quad (23)$$

If $i \in \mathcal{I}^*$ then by Proposition 4 we have

$$\|\mathbf{Z}_i^\top \mathbf{w}^*\|_2 = \sqrt{\mathbf{w}^\top D_i \mathbf{w}} = \|\mathbf{y}_i - \mathbf{R}^* \mathbf{x}_i\|_2 = 0. \quad (24)$$

Hence the difference $h(\mathbf{w}) - h(\mathbf{w}^*)$ is equal to

$$c_0 \sum_{i \in \mathcal{I}^*} \|\mathbf{Z}_i^\top \mathbf{w}_0\|_2 + \sum_{i \in [\ell] \setminus \mathcal{I}^*} \left(\|\mathbf{Z}_i^\top \mathbf{w}\|_2 - \|\mathbf{Z}_i^\top \mathbf{w}^*\|_2 \right).$$

By (23) and the definition of η_{\min} (12), we know that

$$c_0 \sum_{i \in \mathcal{I}^*} \|\mathbf{Z}_i^\top \mathbf{w}_0\|_2 \geq \frac{k^* \eta_{\min} \text{dist}(\mathbf{w}, \pm \mathbf{w}^*)}{\sqrt{2}}. \quad (25)$$

By triangle inequality the second summation in the above the difference $h(\mathbf{w}) - h(\mathbf{w}^*)$ is smaller than or equal to $\sum_{i \in [\ell] \setminus \mathcal{I}^*} \|\mathbf{Z}_i^\top (\mathbf{w} - \mathbf{w}^*)\|_2$, but this bound satisfies

$$\sum_{i \in [\ell] \setminus \mathcal{I}^*} \|\mathbf{Z}_i^\top (\mathbf{w} - \mathbf{w}^*)\|_2 \leq (\ell - k^*) \eta_{\max} \text{dist}(\mathbf{w}, \pm \mathbf{w}^*),$$

where we used $\text{dist}(\mathbf{w}, \pm \mathbf{w}^*) = \sqrt{2 - 2c^*} = \|\mathbf{w} - \mathbf{w}^*\|_2$ (23) and the definition of (13). We finished the proof.

B.2. Probabilistic Interpretation of Proposition 5

B.2.1 Technical Assumptions

We assume there is no noise for two reasons. First, analysis for noisy data is more challenging and requires a full different chapter to penetrate. Second, analysis in the noiseless case typically serves as a starting point for and sheds enough light on analysis for noise. For example, see the trajectory of the development from the noiseless case [85] to the noisy case [30] in the context of DPCP.

Next, we discuss probabilistic assumptions on inliers. For an inlier index $i \in \mathcal{I}^*$, each column of \mathbf{Z}_i lies in the ground-truth hyperplane $\mathcal{S}^* \subset \mathbb{R}^4$ that is perpendicular to the ground-truth unit quaternion $\pm \mathbf{w}^*$, and the two columns of \mathbf{Z}_i span a subspace \mathcal{S}_i of dimension 2 that is contained in \mathcal{S}^* . Note that any $\mathbf{Z}'_i \in \mathbb{R}^{4 \times 2}$ whose columns are in $\mathcal{S}_i \cap \mathbb{S}^3$ are equivalent to \mathbf{Z}_i in the sense that $\|\mathbf{Z}'_i \mathbf{w}^*\|_2 = \|(\mathbf{Z}'_i)^\top \mathbf{w}^*\|_2 = 0$. To impose randomness assumptions on \mathbf{Z}_i , one could simply replace \mathbf{Z}_i by a 4×2 random matrix whose columns are independently sampled uniformly at random from the intersection $\mathcal{S}_i \cap \mathbb{S}^3$. In fact, we need a slightly stronger assumption:

Assumption 1 (*randomness on inliers*). For each $i \in \mathcal{I}^*$, every column of \mathbf{Z}_i is independently sampled uniformly at random from the intersection $\mathcal{S}^* \cap \mathbb{S}^3$.

This assumption destroys some good property of \mathbf{Z}_i : it might not be orthonormal in general. However, it is orthonormal in expectation, i.e., it satisfies $\mathbb{E}[\mathbf{Z}_i^\top \mathbf{Z}_i] = \mathbf{I}_2$. This will suffice for our later analysis.

On the other hand, Assumption 1 simplifies matters by a lot. This can be appreciated in comparison with a “common” approach, where one makes assumptions on the “source data”, which are point pairs $(\mathbf{y}_i, \mathbf{x}_i)$ ’s in our case. Let us first recall the “data flow” from $(\mathbf{y}_i, \mathbf{x}_i)$ to \mathbf{Z}_i :

$$(\mathbf{y}_i, \mathbf{x}_i) \xrightarrow{\text{Proposition 6}} \mathbf{D}_i \xrightarrow{\text{factorizing } \mathbf{D}_i} \mathbf{Z}_i \quad (26)$$

In view of the above flow (or graphical model), one intuitively (not very rigorously) feels that, if $(\mathbf{y}_i, \mathbf{x}_i)$ ’s are independent, then \mathbf{Z}_i ’s are independent; the latter is implied by Assumption 1. On the other hand, it seems hard to know the distribution of \mathbf{Z}_i ’s, even if the distribution of $(\mathbf{y}_i, \mathbf{x}_i)$ ’s is given or assumed. It is via Assumption 1 that this challenge is circumvented and that our theorems are developed.

Finally, we need randomness on outliers:

Assumption 2 (*randomness on outliers*). Each column of any outlier \mathbf{Z}_j , where $j \in [\ell] \setminus \mathcal{I}^*$, is independently sampled uniformly at random from \mathbb{S}^3 .

Since an outlier \mathbf{Z}_j could be distributed arbitrarily, this assumption is the most natural, if not the most challenging, as the outliers try their best to mimic the distribution of inliers. Assumptions 1 and 2 (together with the noiseless assumption) are all we need for the next section.

B.2.2 Probabilistic Interpretation

Recall that the quantities η_{\min}, η_{\max} of interest are equal to

$$\eta_{\min} = \frac{1}{k^*} \min_{\mathbf{w} \in \mathcal{S}^* \cap \mathbb{S}^3} \sum_{i \in \mathcal{I}^*} \|\mathbf{Z}_i^\top \mathbf{w}\|_2, \quad \text{and} \quad (27)$$

$$\eta_{\max} = \frac{1}{\ell - k^*} \max_{\mathbf{w} \in \mathbb{S}^3} \sum_{j \in [\ell] \setminus \mathcal{I}^*} \|\mathbf{Z}_j^\top \mathbf{w}\|_2. \quad (28)$$

The following proposition gives probabilistic upper and lower bounds for η_{\max} and η_{\min} respectively.

Proposition 7. *Under the assumptions of §B.2.1, we have*

(i) *With probability at least $1 - \exp(-\zeta^2/2)$ it holds that*

$$\eta_{\max} \leq \frac{1}{\sqrt{2}} + \frac{(4 + \zeta)}{\sqrt{\ell - k^*}}. \quad (29)$$

(ii) *With probability at least $1 - \exp(-\zeta^2/2)$ it holds that*

$$\eta_{\min} \geq \sqrt{\frac{2}{3}} - \frac{(4 + \zeta)}{\sqrt{k^*}} \quad (30)$$

To prove Proposition 7 (cf. Appendix B.2.3), we combine the proof strategies of [60] and [98], where both sets of the authors found inspirations from [55]. We can now see that the condition of Proposition 5, $\alpha^* := k^* \eta_{\min} / \sqrt{2} - (\ell - k^*) \eta_{\max} > 0$, holds with high probability as long as

$$\sqrt{\frac{2}{3}} k^* - (4 + \zeta) \sqrt{k^*} \geq \frac{1}{\sqrt{2}} (\ell - k^*) + (4 + \zeta) \sqrt{\ell - k^*}.$$

Ignoring lower-order terms we get the condition

$$k^* \gtrsim \frac{\sqrt{3}}{2} (\ell - k^*) \Leftrightarrow \frac{k^*}{\ell} \gtrsim \frac{\sqrt{3}}{\sqrt{3} + 2}, \quad (31)$$

which holds true whenever there are sufficiently many inliers. This condition ensures the α^* -sharpness, from which local linear convergence to $\pm \mathbf{w}^*$ from a good enough initialization with proper stepsize ensues.

B.2.3 Details: Proof of Proposition 7

We need the following simple result, with its proof omitted.

Lemma 2. *If $\mathbf{z} = [z_1, z_2, z_3, z_4]^\top$ sampled uniformly at random from \mathbb{S}^3 , we have for any $\mathbf{w} \in \mathbb{S}^3$ that*

$$\mathbb{E}[(\mathbf{z}^\top \mathbf{w})^2] = \frac{1}{4}. \quad (32)$$

On the other hand, if $\hat{\mathbf{z}}$ is sampled uniformly at random from $\mathbb{S}^3 \cap \mathcal{S}$ where \mathcal{S} is a linear subspace of \mathbb{R}^4 of dimension 3, then we have for every $\hat{\mathbf{w}} \in \mathbb{S}^3 \cap \mathcal{S}$ that

$$\mathbb{E}[(\hat{\mathbf{z}}^\top \hat{\mathbf{w}})^2] = \frac{1}{3}. \quad (33)$$

Upper Bounding η_{\max} (i). We first prove (i) of Proposition 7. Consider matrix $\mathbf{Z} \in \mathbb{R}^{4 \times 2}$ whose columns are sampled independently and uniformly at random from the 3-sphere \mathbb{S}^3 . We will give upper bounds respectively for

$$(\ell - k^*) \max_{\mathbf{w} \in \mathbb{S}^3} \mathbb{E} \left[\|\mathbf{Z}^\top \mathbf{w}\|_2 \right] \quad \text{and} \quad (34)$$

$$\max_{\mathbf{w} \in \mathbb{S}^3} \sum_{j \in [\ell] \setminus \mathcal{I}^*} \left(\|\mathbf{Z}_j^\top \mathbf{w}\|_2 - \mathbb{E} \left[\|\mathbf{Z}^\top \mathbf{w}\|_2 \right] \right), \quad (35)$$

while summing the two bounds gives an upper bound for $(\ell - k^*) \eta_{\max}$. For (34), Jensen’s inequality gives

$$\max_{\mathbf{w} \in \mathbb{S}^3} \mathbb{E} \left[\|\mathbf{Z}^\top \mathbf{w}\|_2 \right] \leq \max_{\mathbf{w} \in \mathbb{S}^3} \sqrt{\mathbb{E} \left[\|\mathbf{Z}^\top \mathbf{w}\|_2^2 \right]} \quad (36)$$

$$= \max_{\mathbf{w} \in \mathbb{S}^3} \sqrt{2 \cdot \frac{1}{4}} = \frac{1}{\sqrt{2}}. \quad (37)$$

To obtain (37) we used (32) and the linearity of the expectation. The second term (35) is harder to handle, and we first

consider its expectation $\mathbb{E}[(35)]$. We know from a standard symmetrization argument (cf. [49], Lemma 11.4 of [17]) that, since \mathbf{Z}_j 's are independent (Assumption 2), the expectation $\mathbb{E}[(35)]$ has the following bound:

$$\mathbb{E}[(35)] \leq 2 \mathbb{E} \left[\max_{\mathbf{w} \in \mathbb{S}^3} \sum_{j \in [\ell] \setminus \mathcal{I}^*} r_j \|\mathbf{Z}_j^\top \mathbf{w}\|_2 \right], \quad (38)$$

where r_j 's are independent Radeamacher random variables which take values 1, -1 with probabilities $1/2$ each and independent of \mathbf{Z}_j 's. We also know from the *vector contraction inequality* (cf. Corollary 1 of [66]) that the right-hand side of (38), and thus $\mathbb{E}[(35)]$, is has the following bound:

$$\begin{aligned} \mathbb{E}[(35)] &\leq 2\sqrt{2} \mathbb{E} \left[\max_{\mathbf{w} \in \mathbb{S}^3} \sum_{j \in [\ell] \setminus \mathcal{I}^*} \left(r_{j1} \mathbf{Z}_{j1}^\top \mathbf{w} + r_{j2} \mathbf{Z}_{j2}^\top \mathbf{w} \right) \right] \\ &= 2\sqrt{2} \mathbb{E} \left[\left\| \sum_{j \in [\ell] \setminus \mathcal{I}^*} \left(r_{j1} \mathbf{Z}_{j1} + r_{j2} \mathbf{Z}_{j2} \right) \right\|_2 \right] \end{aligned} \quad (39)$$

where \mathbf{Z}_{j1} 's and \mathbf{Z}_{j2} 's are the first and second columns of \mathbf{Z}_j respectively, while r_{j1} 's and r_{j2} 's are independent Radeamacher random variables that are also independent of entries of \mathbf{Z}_j 's. Applying Jensen's inequality to (39) we get

$$\begin{aligned} \mathbb{E}[(35)] &\leq 2\sqrt{2} \sqrt{\mathbb{E} \left[\left\| \sum_{j \in [\ell] \setminus \mathcal{I}^*} \left(r_{j1} \mathbf{Z}_{j1} + r_{j2} \mathbf{Z}_{j2} \right) \right\|_2^2 \right]} \\ &= 2\sqrt{2} \sqrt{\mathbb{E} \left[\sum_{j \in [\ell] \setminus \mathcal{I}^*} \left(r_{j1}^2 \mathbf{Z}_{j1}^\top \mathbf{Z}_{j1} + r_{j2}^2 \mathbf{Z}_{j2}^\top \mathbf{Z}_{j2} \right) \right]} \\ &= 4\sqrt{\ell - k^*} \end{aligned}$$

To summarize, we have $\mathbb{E}[(35)] \leq 4\sqrt{\ell - k^*}$. Treat now (35) as a function of \mathbf{Z}_j 's. It is straightforward to verify that this function has *bounded difference 2* (cf. [67]). Since \mathbf{Z}_j 's are independent (Assumption 2), Mcdiarmid's Lemma [67] or the *bounded difference inequality* is applicable, from which we obtain the following probability bound:

$$\mathbb{P} \left((35) \geq \mathbb{E}[(35)] + \zeta_0 \right) \leq \exp \left(- \frac{\zeta_0^2}{2(\ell - k^*)} \right). \quad (40)$$

With $\mathbb{E}[(35)] \leq 4\sqrt{\ell - k^*}$ and $\zeta := \zeta_0 / \sqrt{\ell - k^*}$, we get

$$\mathbb{P} \left((35) \leq (4 + \zeta)\sqrt{\ell - k^*} \right) \geq 1 - \exp \left(- \frac{\zeta^2}{2} \right). \quad (41)$$

Combining this with (37) finishes proving (i).

Lower Bounding η_{\min} (ii). Let $\mathbf{U} \in \mathbb{R}^{4 \times 3}$ have orthonormal columns and have \mathcal{S}^* as its column space, then there is a unique $\mathbf{v} \in \mathbb{S}^2$ so that $\mathbf{U}\mathbf{v} = \mathbf{w}$ for any $\mathbf{w} \in \mathbb{S}^3$. Also, since for any $i \in \mathcal{I}^*$ every column of \mathbf{Z}_i is in \mathcal{S}^* , there

is a unique $\mathbf{A}_i \in \mathbb{R}^{3 \times 2}$ with orthonormal columns satisfying $\mathbf{Z}_i = \mathbf{U}\mathbf{A}_i$. Moreover, by rotation invariance we know that each column of \mathbf{A}_i is uniformly distributed on \mathbb{S}^2 . As a result, we get $\mathbf{Z}_i^\top \mathbf{w} = \mathbf{A}_i^\top \mathbf{v}$, $\forall i \in \mathcal{I}^*$, and η_{\min} is equal to

$$\eta_{\min} = \frac{1}{k^*} \min_{\mathbf{v} \in \mathbb{S}^2} \sum_{i \in \mathcal{I}^*} \|\mathbf{A}_i^\top \mathbf{v}\|_2. \quad (42)$$

Now, lower bounding η_{\min} can be done in a similar way to upper bounding η_{\max} ; thus we only give a proof sketch next. Similarly to (34) and (35), to bound η_{\min} we will find lower bounds respectively for the two terms

$$k^* \min_{\mathbf{v} \in \mathbb{S}^2} \mathbb{E} \left[\|\mathbf{A}^\top \mathbf{v}\|_2 \right] \text{ and} \quad (43)$$

$$\min_{\mathbf{v} \in \mathbb{S}^2} \sum_{i \in \mathcal{I}^*} \left(\|\mathbf{A}_i^\top \mathbf{v}\|_2 - \mathbb{E} \left[\|\mathbf{A}^\top \mathbf{v}\|_2 \right] \right), \quad (44)$$

where \mathbf{A} is an i.i.d. copy of \mathbf{A}_i . Similarly to (37), the first term here is bounded using (33) and Jensen's inequality:

$$\min_{\mathbf{v} \in \mathbb{S}^2} \mathbb{E} \left[\|\mathbf{A}^\top \mathbf{v}\|_2 \right] \leq \sqrt{\frac{2}{3}} \quad (45)$$

Using the symmetric argument, the vector contraction inequality, and Jensen's inequality, the expectation $\mathbb{E}[(44)]$ of the second term (44) is bounded below by $-4\sqrt{k^*}$. Similarly, invoking Mcdiarmid's Lemma gives that

$$\mathbb{P} \left((44) \leq \mathbb{E}[(44)] - \zeta_0 \right) \leq \exp \left(- \frac{\zeta_0^2}{2k^*} \right) \quad (46)$$

$$\Rightarrow \mathbb{P} \left((44) \geq -(4 + \zeta)\sqrt{k^*} \right) \geq 1 - \exp \left(- \frac{\zeta^2}{2} \right) \quad (47)$$

where ζ_0 is any positive constant and we set $\zeta := \zeta_0 / \sqrt{k^*}$. Combining (45) with the above bound finishes the proof.

C. Proof of Proposition 1

Since \mathbf{b}^* is the rotation axis of \mathbf{R}^* , we have $(\mathbf{R}^*)^\top \mathbf{b}^* = \mathbf{b}^*$. Recall $\mathbf{v}_i = \mathbf{y}_i - \mathbf{x}_i$ for every $i \in \mathcal{I}$. If $i \in \mathcal{I}^*$ then

$$\mathbf{v}_i^\top \mathbf{b}^* = (\mathbf{y}_i - \mathbf{x}_i)^\top \mathbf{b}^* = (\mathbf{y}_i - \mathbf{R}^* \mathbf{x}_i)^\top \mathbf{b}^*, \quad (48)$$

and further more if $(\mathbf{y}_i, \mathbf{x}_i)$ is an inlier pair we get that

$$|\mathbf{v}_i^\top \mathbf{b}^*| = \epsilon_i^\top \mathbf{b}. \quad (49)$$

Clearly $\epsilon_i^\top \mathbf{b}$ is a Gaussian random variable with zero mean and variance σ^2 . The rest of the proof follows from a standard probability calculation.

D. Interval Stabbing

Here we provide proofs for Propositions 2 and 3. Along the way we will need multiple temporary variables to illustrate the idea; we use $a_{i,j}$'s to denote those variables. Here,

i denotes the i -th point pair, and j denotes the order in which $a_{i,j}$ appears for the first time. In §4.2.1 we reviewed interval stabbing for closed intervals \mathcal{J}_i of the form $[a, b]$. One should note and verify that this can be easily extended to the case where \mathcal{J}_i is a finite (disjoint) union of closed intervals.

D.1. Proof of Proposition 2

Recall $\mathbf{b} = [\sin(\theta) \cos(\phi), \sin(\theta) \sin(\phi), \cos(\theta)]^\top$ with $\theta \in [0, \pi]$, $\phi \in [0, \pi]$. Denote by $a_{i,1} := [\mathbf{v}_i]_1 \cos(\phi) + [\mathbf{v}_i]_2 \sin(\phi)$, then $|\mathbf{v}_i^\top \mathbf{b}| \leq c$ is equivalent to

$$|a_{i,1} \sin(\theta) + [\mathbf{v}_i]_3 \cos(\theta)| \leq c. \quad (50)$$

Without loss of generality we can assume that $a_{i,1} \geq 0$. So there is a unique $a_{i,2} \in [0, \pi]$ which satisfies

$$\cos(a_{i,2}) = \frac{[\mathbf{v}_i]_3}{\sqrt{[\mathbf{v}_i]_3^2 + a_{i,1}^2}}, \quad \sin(a_{i,2}) = \frac{a_{i,1}}{\sqrt{[\mathbf{v}_i]_3^2 + a_{i,1}^2}}.$$

Hence (50) is equivalent to

$$|\cos(\theta - a_{i,2})| \leq c_i, \quad c_i := \min \left\{ 1, \frac{c}{\sqrt{[\mathbf{v}_i]_3^2 + a_{i,1}^2}} \right\}$$

Since the trigonometric function $\arccos : [0, \pi] \rightarrow [-1, 1]$ is decreasing and $|\theta - a_{i,2}| \leq \pi$, the above is equivalent to

$$a_{i,3} := \arccos(-c_i) \geq |\theta - a_{i,2}| \geq \arccos(c_i) =: a_{i,4}.$$

Define $a_{i,5} = a_{i,2} - a_{i,3}$, $a_{i,6} = a_{i,2} - a_{i,4}$, $a_{i,7} = a_{i,2} + a_{i,4}$, and $a_{i,8} = a_{i,2} + a_{i,3}$. Then $|\mathbf{v}_i^\top \mathbf{b}| \leq c$ is the same as

$$\theta \in ([a_{i,5}, a_{i,6}] \cup [a_{i,7}, a_{i,8}]) \cap [0, \pi] \quad (51)$$

To summarize, given $\phi \in [0, \pi]$, the i -th constraint of (5) requires θ to lie in the union of some disjoint intervals defined in (51). So maximizing (6) amounts to finding a maximal set of intervals of the form (51) that overlap a point θ , and can be solved by interval stabbing in $O(\ell \log \ell)$ time.

D.2. Proof of Proposition 3

Assume that the rotation axis \mathbf{b} of the 3D rotation

$$\mathbf{R} = \mathbf{b}\mathbf{b}^\top + [\mathbf{b}]_\times \sin(\omega) + (\mathbf{I}_3 - \mathbf{b}\mathbf{b}^\top) \cos(\omega) \quad (52)$$

is given, and we now solve (7). Let $a_{i,9} = \mathbf{y}_i^\top \mathbf{b}\mathbf{b}^\top \mathbf{x}_i$, $a_{i,10} = \mathbf{y}_i^\top [\mathbf{b}]_\times \mathbf{x}_i$ and $a_{i,11} = \mathbf{y}_i^\top (\mathbf{I}_3 - \mathbf{b}\mathbf{b}^\top) \mathbf{x}_i$. Then

$$\mathbf{y}_i^\top \mathbf{R} \mathbf{x}_i = a_{i,9} + a_{i,10} \sin(\omega) + a_{i,11} \cos(\omega). \quad (53)$$

Hence the constraint of (4) can be written as

$$\|\mathbf{y}_i\|_2^2 + \|\mathbf{x}_i\|_2^2 - c^2 \leq 2\mathbf{y}_i^\top \mathbf{R} \mathbf{x}_i \quad (54)$$

$$\Leftrightarrow a_{i,10} \sin(\omega) + a_{i,11} \cos(\omega) \geq a_{i,12} \quad (55)$$

where we defined $a_{i,12} = (\|\mathbf{y}_i\|_2^2 + \|\mathbf{x}_i\|_2^2 - c^2)/2 - a_{i,9}$. There is a unique angle $a_{i,13} \in [0, 2\pi)$ satisfying

$$\cos(a_{i,13}) = \frac{a_{i,11}}{\sqrt{a_{i,10}^2 + a_{i,11}^2}}, \quad \sin(a_{i,13}) = \frac{a_{i,10}}{\sqrt{a_{i,10}^2 + a_{i,11}^2}}$$

Thus, the constraint $\|\mathbf{y}_i - \mathbf{R} \mathbf{x}_i\|_2 \leq c$ of (4) is the same as

$$\cos(\omega - a_{i,13}) \geq \max \left\{ \frac{a_{i,12}}{\sqrt{a_{i,10}^2 + a_{i,11}^2}}, -1 \right\} =: a_{i,14}.$$

Without loss of generality assume $a_{i,14} \leq 1$, for otherwise we could simply ignore this constraint. Define $a_{i,15} = \arccos(a_{i,14}) \in [0, \pi]$. Since $|\omega - a_{i,13}| \in [0, 2\pi]$, we consider two cases, namely $|\omega - a_{i,13}| \leq \pi$ and $|\omega - a_{i,13}| > \pi$. In the former case, since \arccos is a decreasing function, the above constraint is equivalent to $|\omega - a_{i,13}| \leq a_{i,15}$. In the later case the above constraint is equivalent to

$$\cos(2\pi - |\omega - a_{i,13}|) \geq a_{i,14} \Leftrightarrow 2\pi - |\omega - a_{i,13}| \leq a_{i,15}.$$

Thus, the constraint $\|\mathbf{y}_i - \mathbf{R} \mathbf{x}_i\|_2 \leq c$ of (4) requires $\omega \in [0, 2\pi]$ to lie in the union of the following intervals.

$$[a_{i,13} - a_{i,15}, a_{i,13} + a_{i,15}] \cap [0, 2\pi] \quad (56)$$

$$[a_{i,13} - a_{i,15} + 2\pi, 2\pi] \quad (57)$$

$$[0, a_{i,13} + a_{i,15} - 2\pi]. \quad (58)$$

In the above, the invalid interval where the right endpoint is smaller than its left endpoint, if any, should be discarded. To conclude, (7) can be solved via interval stabbing.

E. More Experiments

In this section we present more experiments. Besides rotation errors, we will also use another metric for evaluation, that is *success rate*. Given two point clouds as input, an algorithm *succeeds* if it outputs a rotation that has error smaller than a certain threshold; by default the threshold is set to 10 degree (as in [91]) but we will also vary it when appropriate. The success rate is the number of success divided by the total number of experiments that were run. This metric was referred to as *recall* in other related papers (cf. [25]).

Note that, like GORE [19] and QUASAR [88], ARCS_{OR} can be applied to image stitching, because sometimes the translation is negligible and thus the scene can be justified by a homography $\mathbf{H} \in \mathbb{R}^{3 \times 3}$ that involves a pure 3D rotation \mathbf{R} , i.e., $\mathbf{H} = \mathbf{K} \mathbf{R} \mathbf{K}^{-1}$ (cf. [83]); here $\mathbf{K} \in \mathbb{R}^{3 \times 3}$ is a matrix of intrinsic camera parameters given by the dataset. However, we noticed that the recent approaches MAGSAC++ [7–9] and VSAC [45] achieved surprising performance and run in fewer than 10 milliseconds for image stitching, hence we would recommend them for this task.

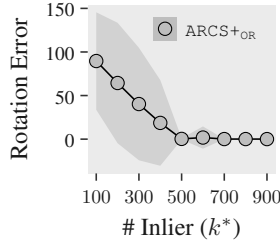


Figure 3. Performance of ARCS+OR on Gaussian point sets with $\ell = 10^7$ point pairs, $\sigma = 0.01$, 100 trials. ARCS+OR works well until there are fewer than $500/10^7 = 0.005\%$ inliers.

E.1. Robustness on Gaussian Point Sets

In previous synthetic experiments on robust rotation search (Table 4), we generated data by ensuring that each point pair \mathbf{y}_i and \mathbf{x}_i has nearly the same norm. This is for fair comparison of the methods, and it might not be true in practice. Here we show that, without this norm constraint, ARCS+OR can tolerate even more outliers. In the experiment here we generated point sets $\{\mathbf{y}_i, \mathbf{x}_i\}_{i=1}^{\ell}$ as in Table 4 except without the norm constraint. Then, we first perform a simple step, that removes all point pairs $(\mathbf{y}_i, \mathbf{x}_i)$ which satisfy $|\|\mathbf{y}_i\|_2 - \|\mathbf{x}_i\|_2| > c$, and then feed the remaining points to ARCS+OR. We reported the results in Figure 3, where we observed that ARCS+OR worked well until there are fewer than $500/10^7 = 0.005\%$ inliers.

E.2. Sensitivity to The Ground-Truth Rotation

In Figure 4 we presented the sensitivity of ARCS+OR to the ground-truth rotation \mathbf{R}^* . Figure 4a depicted that, with the ground-truth rotation angle ω^* changing, the mean estimation error of ARCS+O varied from 0.5 to 1, while the standard deviation ranged from 0 to 0.5. On the other hand, ARCS+R refined the estimate from ARCS+O, so that their combination ARCS+OR had much smaller mean error and standard deviation, nearly imperceptible from Figure 4a. In Figure 4b we kept ω^* fixed and presented how the errors of ARCS+OR vary with θ^* and ϕ^* , the two angles for the ground-truth rotation axis \mathbf{b}^* ; we fixed one of them when varying the other. We observed that ARCS+OR is immune to the change of ϕ^* , as it consistently gave about 0.02 errors and 0.01 standard deviation. This is expected as ARCS+O selects from multiple ϕ_j 's a best one based on consensus maximization. On the other hand, varying ϕ^* does make an impact on the performance of ARCS+OR; the standard deviation reached its peak, around 0.04, when $\theta^* = \pi/4$. Theoretically justifying the phenomenon presented here can be an interesting future work.

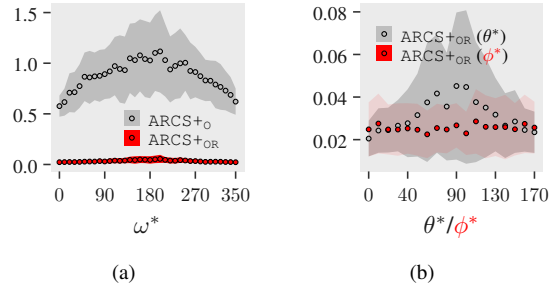


Figure 4. Average rotation errors (in degrees) and standard deviations with respect to the ground-truth rotation angle ω^* and axis $\mathbf{b}^* = [\sin(\theta^*) \cos(\phi^*), \sin(\theta^*) \sin(\phi^*), \cos(\theta^*)]^T$. Experiments run with 100 trials, $\ell = 10^5$, $k^* = 1000$, $\sigma = 0.01$.

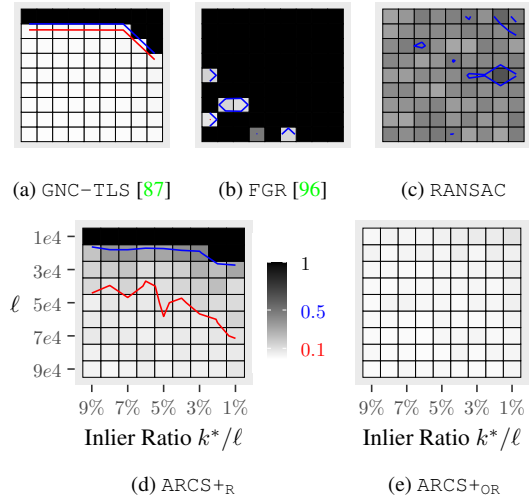


Figure 5. Average rotation errors in degrees of different robust rotation search approaches on medium-scale synthetic 3D point sets of sizes varying from 10^4 to 9×10^4 with inlier ratios ranging from 1% to 9%. Experiments run with 50 trials, $\sigma = 0.01$ fixed.

E.3. Phase Transition

In Figure 5, we showed the performances of algorithms for different inlier ratios k^*/ℓ and different number ℓ of points; whiter means smaller errors and errors larger than 1 were truncated to 1. The major point we would like to clarify here is that, whether or not an algorithm can tolerate say 99% outliers might depend on the total number of points (cf. Figures 5a and 5d), so sentences such as “our algorithm can tolerate 99% outliers” might be inaccurate, even though such description has been widely used in recent papers. Indeed, no algorithm can tolerate 99% outliers if $\ell = 100$. Also, as mentioned in §4.3, one theorem of [16] has shed light on this phenomenon. The other important observation here is that, GNC-TLS achieved higher accuracy than ARCS+R, although they exhibited nearly the same breaking

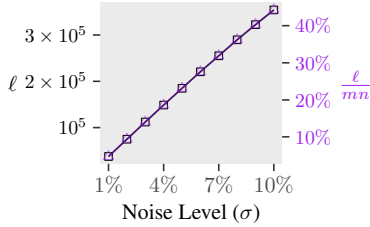


Figure 6. Sensitivity of $\text{ARCS}+\text{N}$ to noise: ℓ increases linearly as σ grows. 100 trials, $m = 1000$, $n = 800$, $k^* = 200$, $c = 5.54\sigma$.

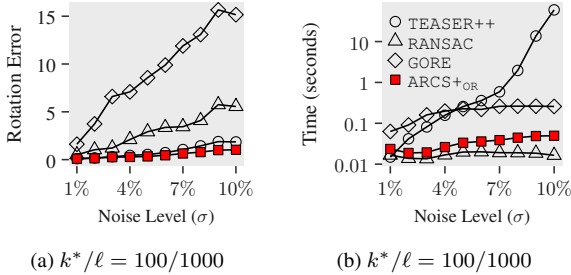


Figure 7. Robustness of various methods to noise. 20 trials.

down points. One reason is that GNC-TLS takes advantage of the inlier threshold c as extra information. This empirically suggests that combining $\text{ARCS}+\text{O}$ and GNC-TLS might further boost the performance for robust rotation search.

E.4. Robustness to Noise

Figure 6 showed that $\text{ARCS}+\text{N}$ is sensitive to noise: In particular, for $c = 5.54\sigma$ fixed, the number ℓ of output point pairs grows proportionally as a linear function of σ . A similar phenomenon can be found in [91] and its follow-up works: Higher noise leads to denser graphs, and thus to intractable maximal clique problems (recall Section 1).

However, $\text{ARCS}+\text{O}$ and $\text{ARCS}+\text{OR}$ behave reasonably well as noise varies. This was shown in Figure 7, where we observed that, for $k^*/\ell = 100/1000$, $\text{ARCS}+\text{OR}$ are competitive to $\text{TEASER}++$ in terms of accuracy (Figure 7a) and to RANSAC in terms of speed (Figure 7b); 10% inliers are enough for RANSAC to be fast. Also note that the running time of $\text{TEASER}++$ increases exponentially as noise grows, and that GORE would achieve higher accuracy if some local refinement methods were applied.

E.5. Procrustes’s Experiments on Stanford Bunny

Here we use $\text{ARCS}+$ for simultaneous search of rotation & correspondences on a popular benchmark, the Stanford Bunny dataset [27].⁸ Bunny has 35947 points with every coordinate of the points located in $[-1, 1]$ (Figure 8a). We randomly cut it into two parts, \mathcal{Q} and \mathcal{P} , of sizes

⁸In view of our opening quote, Bunny here is a victim of Procrustes.

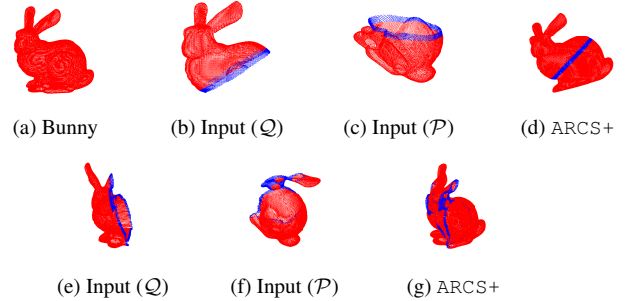


Figure 8. Bunny (8a) was cut through its body into two parts, \mathcal{Q} (8b) and \mathcal{P} (8c), with $k^*/m = 1997/19970 = 10\%$ overlapping points in blue. \mathcal{P} was randomly rotated and corrupted by 1% random noise. $\text{ARCS}+$ successfully aligned \mathcal{Q} and \mathcal{P} (8d). For a different cut through the ear of Bunny (8e-8f), $\text{ARCS}+$ failed (8g).

m and n respectively and of different overlapping ratios $k^*/\max\{m, n\} = k^*/m$ (Figures 8b-8c or 8e-8f). For simplicity we set $n = \lceil 35947/2 \rceil = 17974$ and, $m = \lceil 35947/2 \rceil + k^*$, so the exact values of m and k^* can be calculated as per a given overlapping ratio k^*/m . We then randomly rotated \mathcal{P} and added 1% random Gaussian noise to it. The goal is to align \mathcal{P} and \mathcal{Q} . $\text{ARCS}+$ can be applied directly to this task (Figures 8d or 8g). For comparison, we gave GORE and $\text{TEASER}++$ the correspondences established by FPFH . For all methods we set $c = 5 \times 10^{-5}$. Figure 9 showed the results for different overlapping ratios, from which we made a few observations: $\text{ARCS}+$ achieved higher success rates in all experiments, while the performance of FPFH , and thus of $\text{TEASER}++$ and GORE , improved as the overlapping ratios increased. We did not put RANSAC into comparison here, because FPFH often gave few to none inlier pairs for small k^*/m and so RANSAC used much longer time to reach a confidence of 0.99.

F. Handling The Translation Case

Utilizing ideas that have been known in prior works, it is easy to extend our algorithms to the situation where there is an extra unknown translation. As we did for Problems 1 and 2, we first define the two problems that we will discuss:

Problem 3 (simultaneous pose and correspondences). Let the two point sets \mathcal{Q} and \mathcal{P} of Problem 1 instead satisfy

$$\mathbf{q}_i = \mathbf{R}^* \mathbf{p}_j + \mathbf{t}^* + \mathbf{o}_{i,j} + \boldsymbol{\epsilon}_{i,j}, \quad (59)$$

where $\mathbf{t}^* \in \mathbb{R}^3$ is an extra unknown translation vector. The task is to simultaneously estimate the rotation \mathbf{R}^* , translation \mathbf{t}^* , and correspondences \mathcal{C}^* from \mathcal{Q} and \mathcal{P} .

Problem 4 (robust registration). Let the ℓ pairs of 3D points $\{(\mathbf{y}_i, \mathbf{x}_i)\}_{i=1}^{\ell}$ of Problem 2 instead satisfy

$$\mathbf{y}_i = \mathbf{R}^* \mathbf{x}_i + \mathbf{t}^* + \mathbf{o}_i + \boldsymbol{\epsilon}_i. \quad (60)$$

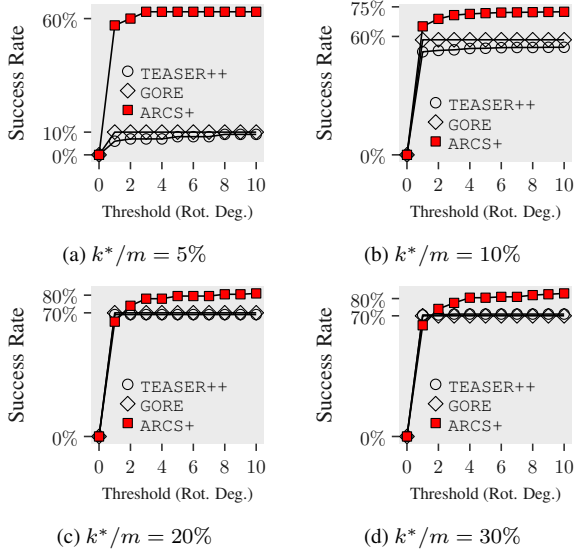


Figure 9. Success Rates of the methods on Stanford Bunny with different overlapping ratios k^*/m . 1000 trials. In each trial, Bunny was randomly cut into two parts \mathcal{Q} and \mathcal{P} , and \mathcal{P} was then rotated randomly and corrupted by 1% random Gaussian noise.

The task is to find \mathbf{R}^* , \mathbf{t}^* , and correspondences \mathcal{I}^* .

We will discuss more about Problem 3 in our future work; here we focus on the its special case, Problem 4. Specifically, we next extend our ARCS+_{OR} algorithm to handle Problem 4 (Appendix F.1), and present its performance on the 3DMatch dataset [95] (Appendix F.2).

F.1. Extension for Robust Registration

Here we present an extension of our ARCS+_{OR} algorithm for solving Problem 4. In this extension, we essentially combine ARCS+_{OR} with *known* techniques. Thus, the presentation here serves more as an useful demonstration of concepts, and less as an entirely novel insight into, or the most efficient method for, solving Problem 4. Nevertheless, we will show in Appendix F.2 that our extension does enjoy state-of-the-art performance on the 3DMatch dataset [95].

We first review three crucial ingredients that are useful for solving Problem 4: *translation elimination (TE)*, *rotation elimination (RE)*, and *outlier removal*.

Translation Elimination (TE). For each $i, j \in [\ell]$, $i > j$, define $\mathbf{y}_{ij} = \mathbf{y}_i - \mathbf{y}_j$ and $\mathbf{x}_{ij} = \mathbf{x}_i - \mathbf{x}_j$, then

$$\mathbf{y}_{ij} = \mathbf{R}^* \mathbf{x}_{ij} + (\mathbf{o}_i - \mathbf{o}_j) + (\boldsymbol{\epsilon}_i - \boldsymbol{\epsilon}_j). \quad (61)$$

Here $(\mathbf{y}_{ij}, \mathbf{x}_{ij})$ is referred to in the literature as *translation invariant measurements*, as (61) no longer involves translation. As a consequence, robust rotation search might be performed over $\{(\mathbf{y}_{ij}, \mathbf{x}_{ij})\}_{i>j}$, yielding an estimate of rotation and correspondences. After this, the translation can

be easily computed. A disadvantage here is that computing all $(\mathbf{y}_{ij}, \mathbf{x}_{ij})$'s needs $O(\ell^2)$ time; also note though that this computation can be implemented in parallel and thus can be efficient for medium-size datasets (e.g., $\ell \leq 3 \times 10^4$).

Rotation Elimination (RE). Every inlier $(\mathbf{y}_i, \mathbf{x}_i)$ satisfying (60) with $\mathbf{o}_i = 0$ also necessarily satisfies

$$\|\mathbf{x}_i + \boldsymbol{\epsilon}_i\|_2 = \|\mathbf{y}_i - \mathbf{t}^*\|_2 \Leftrightarrow \|\mathbf{x}_i\|_2 \approx \|\mathbf{y}_i - \mathbf{t}^*\|_2. \quad (62)$$

If there were no outliers, estimating \mathbf{t}^* from relation (62) is the problem of *source localization* that appears in signal processing applications [13]. Estimating translation from (62) in the presence of outliers is more challenging. A possible algorithm is combining the least-squares solvers of [13] with an iterative reweighting strategy, but this does not have global optimality guarantee. The other approach, which we employ, is to estimate \mathbf{t}^* via branch & bound, solving the following optimization problem:

$$\max_{\mathcal{I} \subset [\ell], \mathbf{t} \in \mathbb{R}^3} |\mathcal{I}| \quad (63)$$

$$\text{s.t.} \quad \|\mathbf{y}_i - \mathbf{t}\|_2 - \|\mathbf{x}_i\|_2 \leq c, \quad \forall i \in \mathcal{I}$$

If directly applying branch & bound to (63), one would branch over \mathbb{R}^3 (cf. [62]). On the other hand, our development in §4.2 implies that branching over \mathbb{R}^2 , where the first two coordinates of \mathbf{t} lie, suffices, as the third coordinate can be determined by interval stabbing. In short, we solve (63) via branching over the two-dimensional space \mathbb{R}^2 if needed. As a matter of fact, branch & bound runs much faster even if the parameter space has smaller dimension.

Remark 4 (TE versus RE). Translation elimination (TE) yields $O(\ell^2)$ measurements, leads to the problem of robust rotation search, and is also used in the 2D-3D *perspective-three-point* problem (see, e.g., [74]); many recent papers on 3D-3D registration used TE (see, e.g., [91] and its follow-up works). RE yields $O(\ell)$ measurements, leads to a less familiar problem, and receives fewer attention; [62] is the only paper, which we know, that uses RE (for Problem 3).

Outlier Removal. Even though rotation or translation can be estimated independently of each other (using TE or RE respectively), they might not be able to handle the case of extreme outlier rates. In particular, if using TE then the inlier ratio decreases from k^*/ℓ to $O((k^*/\ell)^2)$. This is why an outlier removal procedure is needed prior to estimation. For this, create (in mind) a graph \mathcal{G} with ℓ vertices representing the ℓ point pairs $\{(\mathbf{y}_i, \mathbf{x}_i)\}_{i=1}^{\ell}$. Moreover, create an edge between two vertices i and j , if $|\mathbf{y}_{ij} - \mathbf{x}_{ij}| \leq 2c$, where \mathbf{y}_{ij} and \mathbf{x}_{ij} are defined in (61). Then, find a maximum clique of \mathcal{G} , and remove all point pairs whose corresponding vertices are not contained in the maximum clique. See [71, 79, 91] for more transparent discussion on this idea.

For implementation, we use the code of [71] to create \mathcal{G} and compute a maximum clique of it.

Table 6. Two Extensions of ARCS++_{OR} for Problem 4.

	$(\text{ARCS++}_{\text{OR}})^{\text{TE}}$	$(\text{ARCS++}_{\text{OR}})^{\text{RE}}$
Step 1	Outlier Removal	
Step 2	TE	RE
Step 3	ARCS++ _{OR} (61)	Branch & Bound (63)
Step 4	—	ARCS++ _{OR}
Step 5	Local Refinement (optional)	

Algorithms. Having reviewed the three ingredients, we are ready to extend ARCS++_{OR} for Problem 4. We have two extensions, $(\text{ARCS++}_{\text{OR}})^{\text{TE}}$ and $(\text{ARCS++}_{\text{OR}})^{\text{RE}}$, summarized in Table 6. Both of them have the same first step, outlier removal via finding a maximum clique from the constructed graph. Their next steps proceed by working with point pairs that survive from outlier removal. Step 2 of $(\text{ARCS++}_{\text{OR}})^{\text{TE}}$ is to eliminate the translation (TE), and step 3 is to estimate the rotation via ARCS++_{OR} from the point pairs $\{(\mathbf{y}_{ij}, \mathbf{x}_{ij})\}_{i>j}$ (61). Step 4 of $(\text{ARCS++}_{\text{OR}})^{\text{TE}}$ would estimate the translation from the remaining point pairs, with an estimated rotation given by ARCS++_{OR}. But we leave step 4 unspecified, as translation estimation in this situation is straightforward. On the other hand, step 2 of $(\text{ARCS++}_{\text{OR}})^{\text{RE}}$ is to eliminate the rotation (RE), step 3 is to compute a translation $\hat{\mathbf{t}}$ by solving (63), and step 4 is to estimate the rotation via ARCS++_{OR}, operating on point pairs $(\mathbf{y}_i - \hat{\mathbf{t}}, \mathbf{x}_i)$'s. Finally, one might use an extra step 5, to refine the solution, *e.g.*, by singular value decomposition.

F.2. Experiments on 3DMatch

Data. The 3DMatch dataset [95] contains more than 1000 point clouds for testing, representing 8 different scenes (such as kitchen, hotel, etc.), while the number of point clouds for each scene ranges from 77 to 506. Each point cloud has more than 10^5 points, yet in [95] there are 5000 keypoints for each cloud. We used the pretrained model⁹ of the 3DSmoothNet [35] to extract descriptors from these key points, and matched them using the Matlab function `pmatchfeatures`, with its parameter `MatchThreshold` set to the maximum 1. It remains to solve Problem 4 using these hypothetical correspondences.

Metrics. We report success rates of the methods. Success rates were defined in the beginning of Appendix E. The default threshold 10 on rotation degrees is the one that was used in TEASER++ [91]. We do not report errors in terms of translation for two reasons: i) rotation search is the main theme of the paper, ii) if the rotation is estimated accurately, then so will be the translation (see, *e.g.*, algorithms of [91]).

Methods. We apply $(\text{ARCS++}_{\text{OR}})^{\text{TE}}$ and $(\text{ARCS++}_{\text{OR}})^{\text{RE}}$ to restore the rotation and translation from these correspon-

⁹<https://github.com/zgojcic/3DSmoothNet>

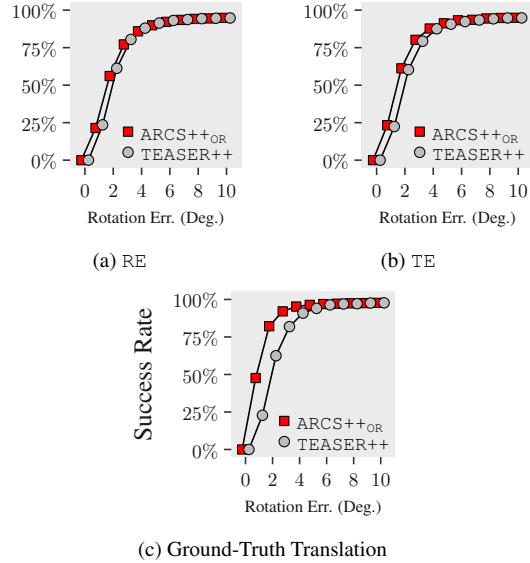


Figure 10. Success rates of TEASER++ and ARCS++_{OR} on the 3D Match dataset, using either estimated translation (Fig. 10a) or TIMs (Fig. 10b) or ground-truth translation (Fig. 10c).

dences. We use singular value decomposition as an extra step 5 for $(\text{ARCS++}_{\text{OR}})^{\text{RE}}$ to refine the solution and account for inaccuracy of translation estimation via branch & bound (63). For reference, we also apply $(\text{ARCS++}_{\text{OR}})^*$, which uses the ground-truth translation \mathbf{t}^* and point pairs $(\mathbf{y}_i - \mathbf{t}^*, \mathbf{x}_i)$'s to estimate a rotation via ARCS++_{OR}.

We compare our algorithms with TEASER++ [91]. Similarly, we use three versions of TEASER++. The first version is $(\text{TEASER++})^{\text{TE}}$. This is the standard TEASER++, and the difference between $(\text{TEASER++})^{\text{TE}}$ and $(\text{ARCS++}_{\text{OR}})^{\text{TE}}$ is that, $(\text{TEASER++})^{\text{TE}}$ estimates the rotation by GNC-TLS, not ARCS++_{OR}. The second version is $(\text{TEASER++})^{\text{TE}}$, where we treat TEASER++ as a robust rotation search method and let it play the role of ARCS++_{OR} in $(\text{ARCS++}_{\text{OR}})^{\text{RE}}$. The third version is $(\text{TEASER++})^*$, where we assume the ground-truth translation \mathbf{t}^* is given and run TEASER++ on $(\mathbf{y}_i - \mathbf{t}^*, \mathbf{x}_i)$'s. Finally, we did not compare other methods here, as TEASER++ currently has the best performance (to the best of our knowledge) on the 3DMatch dataset, see [91] for comparison with optimization-based methods, and also read from [25] the success rates (recall) of other deep learning methods.

Results. Following [91], we set $c = 0.05$. We presented results in Table 7 and Figure 10. In Table 7 we observed that ARCS++_{OR} and TEASER++ have very close performance, although ARCS++_{OR} has slight advantage (*e.g.*, in 12 cases in bold ARCS++_{OR} has higher success rates). In terms of running times, ARCS++_{OR} is slower than TEASER++. One reason is that we used an industrial-strength implementa-

Table 7. Success rates of methods run on the scene pairs of the 3DMatch dataset [95] for which the ground-truth transformations are provided (rotation error smaller than 10 degree means a success [91]; see also the first paragraph of Appendix E).

Scene Type # Scene Pairs	Kitchen 506	Home 1 156	Home 2 208	Hotel 1 226	Hotel 2 104	Hotel 3 54	Study Room 292	MIT Lab 77	Overall 1623
(TEASER++) ^{TE}	98.4%	92.9%	89.9%	98.2%	92.3%	94.4%	93.2%	88.3%	94.82%
(TEASER++) ^{RE}	99.0%	92.3%	89.4%	98.7%	91.3%	94.4%	92.5%	88.3%	94.76%
(TEASER++) [*]	99.0%	98.1%	94.7%	98.7%	99.0%	98.1%	97.0%	94.8%	97.72%
(ARCS++ _{OR}) ^{TE}	98.6%	92.3%	90.4%	98.7%	93.3%	94.4%	92.5%	88.3%	94.89%
(ARCS++ _{OR}) ^{RE}	98.4%	91.7%	89.9%	99.1%	94.2%	94.4%	92.5%	88.3%	94.82%
(ARCS++ _{OR}) [*]	98.4%	97.4%	95.7%	98.7%	98.1%	100%	97.3%	96.1%	97.72%

tion¹⁰ of TEASER++, while ARCS++_{OR} was implemented in plain Matlab. This suggests our current idea of extending ARCS_{OR} into the translation case might be sub-optimal, and will motivate us to design even faster algorithms for that purpose, which though will require serious innovations. Finally, in Figure 10, we reported the success rates averaged over all testing scenes of 3DMatch and with the threshold (rotation degree) varying from 0 to 100. This delivers the same message that our direct extension of ARCS_{OR} maintains a state-of-the-art performance for solving Problem 4.

¹⁰<https://github.com/MIT-SPARK/TEASER-plusplus>